Centrality, rapidity and transverse momentum dependence of J/ψ suppression in Pb–Pb collisions at √sNN = 2.76 TeV

(ALICE Collaboration) Abelev, B.; ...; Antičić, Tome; ...; Gotovac, Sven; ...; Mudnić, Eugen; ...; Planinić, Mirko; ...; ...

Source / Izvornik: **Physics Letters B, 2014, 734, 314 - 327**

Journal article, Published version
Rad u časopisu, Objavljena verzija rada (izdavačev PDF)

https://doi.org/10.1016/j.physletb.2014.05.064

Permanent link / Trajna poveznica: https://urn.nsk.hr/urn:nbn:hr:217:914401

Rights / Prava: Attribution 3.0 Unported/Imenovanje 3.0

Download date / Datum preuzimanja: **2025-04-01**

Repository / Repozitorij:

Repository of the Faculty of Science - University of Zagreb

Physics Letters B 734 (2014) 314–327

Contents lists available at ScienceDirect

Physics Letters B

www.elsevier.com/locate/physletb

Centrality, rapidity and transverse momentum dependence of J/ψ suppression in Pb–Pb collisions at $\sqrt{s_{NN}} = 2.76$ TeV

ALICE Collaboration *

ARTICLE INFO

Article history:
Received 3 November 2013
Received in revised form 15 May 2014
Accepted 20 May 2014
Available online 27 May 2014
Editor: L. Rolandi

Keywords:
Relativistic heavy ion collisions
Quark gluon plasma
Quarkonium
J/ψ suppression
Experimental results

ABSTRACT

The inclusive J/ψ nuclear modification factor (R_{AA}) in Pb–Pb collisions at $\sqrt{s_{NN}} = 2.76$ TeV has been measured by ALICE as a function of centrality in the e^+e^- decay channel at mid-rapidity ($|y| < 0.8$) and as a function of centrality, transverse momentum and rapidity in the $\mu^+\mu^-$ decay channel at forward-rapidity ($2.5 < y < 4$). The J/ψ yields measured in Pb–Pb are suppressed compared to those in pp collisions scaled by the number of binary collisions. The R_{AA} integrated over a centrality range corresponding to 90% of the inelastic Pb–Pb cross section is $0.72 \pm 0.06(\text{stat.}) \pm 0.10(\text{syst.})$ at mid-rapidity and $0.58 \pm 0.01(\text{stat.}) \pm 0.09(\text{syst.})$ at forward-rapidity. At low transverse momentum, significantly larger values of R_{AA} are measured at forward-rapidity compared to measurements at lower energy. These features suggest that a contribution to the J/ψ yield originates from charm quark (re)combination in the deconfined partonic medium.

© 2014 The Authors. Published by Elsevier B.V. This is an open access article under the CC BY license (http://creativecommons.org/licenses/by/3.0/). Funded by SCOAP[3].

1. Introduction

The theory of Quantum Chromodynamics (QCD) predicts that the hot and dense nuclear matter produced during the collision of ultra-relativistic heavy nuclei behaves as a deconfined Plasma of Quarks and Gluons (QGP). This phase of matter exists for only a short time before the fireball cools down and the process of hadronization takes place. Heavy quarks are an important probe of the QGP since they are expected to be produced only during the initial stage of the collision in hard partonic interactions, thus experiencing the entire evolution of the system. It was predicted that in a hot and dense deconfined medium like the QGP, bound states of charm (c) and anti-charm ($\bar{c}$) quarks, i.e. charmonia, are suppressed due to the screening effects induced by the high density of color charges [1]. The relative production probabilities of charmonium states with different binding energies may provide important information on the properties of this medium and, in particular, on its temperature [2,3]. Among the charmonium states, the strongly bound J/ψ is of particular interest. The J/ψ production is a combination from prompt and non-prompt sources. The prompt J/ψ yield consists of the sum of direct J/ψ ($\approx 65\%$) and excited $c\bar{c}$ states such as χ_c and $\psi(2S)$ decaying into $J/\psi + X$ ($\approx 35\%$) [4]. These excited states have a smaller binding energy than the J/ψ. Non-prompt J/ψ production is directly related to beauty hadron production whose relative contribution increases with the energy of the collision. Experimentally, J/ψ production was studied in heavy-ion collisions at the Super Proton Synchrotron (SPS) and at the Relativistic Heavy Ion Collider (RHIC), covering a large energy range from about 20 to 200 GeV center-of-mass energy per nucleon pair ($\sqrt{s_{NN}}$). A suppression of the inclusive J/ψ yield in nucleus–nucleus (A–A) collisions with respect to the one measured in proton–proton (pp) scaled by the number of binary nucleon–nucleon collisions was observed. In the most central events, the suppression is beyond the one induced by cold nuclear matter effects (CNM), such as shadowing and nuclear absorption, at both SPS [5,6] and RHIC [7]. At the SPS the J/ψ suppression is compatible with the melting of the excited states whereas the RHIC data suggest a small amount of suppression for the direct J/ψ [8,9]. Similar predictions on sequential suppression [3] were made for the bottomonium family, which has become accessible at the Large Hadron Collider (LHC) energies. The sequential suppression of the $\Upsilon(1S)$, $\Upsilon(2S)$ and $\Upsilon(3S)$ states was first observed by the CMS experiment in Pb–Pb collisions at $\sqrt{s_{NN}} = 2.76$ TeV [10].

The first ALICE measurement of the inclusive J/ψ production in central Pb–Pb collisions at $\sqrt{s_{NN}} = 2.76$ TeV at forward-rapidity has shown less suppression compared to PHENIX results in central Au–Au collisions at $\sqrt{s_{NN}} = 0.2$ TeV [11]. At $\sqrt{s_{NN}} = 2.76$ TeV, the charm quark density produced in the collisions increases with respect to SPS and RHIC energies [12]. This may result in the enhancement of the probability to create J/ψ mesons from (re)combination of charm quarks [13,14]. If the J/ψ mesons are fully suppressed in the QGP, their creation will take place at chemical freeze-out (near the phase boundary) as detailed in [13,15,16]. If J/ψ mesons survive in the QGP, production may take place continuously during the QGP lifetime [14,17,18]. Because of the

* For correspondence, please use e-mail address: alice-publications@cern.ch.

http://dx.doi.org/10.1016/j.physletb.2014.05.064
0370-2693/© 2014 The Authors. Published by Elsevier B.V. This is an open access article under the CC BY license (http://creativecommons.org/licenses/by/3.0/). Funded by SCOAP[3].

large increase of the $c\bar{c}$ cross-section towards LHC energy the (re)combination mechanism may become dominant there. According to statistical [13] and partonic transport [17,18] models, this contribution leads to an increase of the R_{AA} at the LHC with respect to the one observed at RHIC. In particular, this scenario predicts an increase of the R_{AA} from forward- to mid-rapidity, where the density of charm quarks is higher. Furthermore, in order to (re)combine, two charm quarks need to be close enough in phase space, so that low transverse momentum J/ψ production is expected to be favored. The transverse momentum and rapidity dependence of the J/ψ R_{AA} are therefore crucial observables to sharpen the interpretation of the results, providing a deeper insight on the balance between J/ψ (re)combination and suppression.

In this Letter, we present results on the nuclear modification factor for inclusive J/ψ in Pb–Pb collisions at $\sqrt{s_{NN}} = 2.76$ TeV as a function of collision centrality, transverse momentum and rapidity. Complementary to our results, J/ψ suppression at large transverse momentum in Pb–Pb collisions, was reported previously by ATLAS [19] and CMS [20].

2. Experimental apparatus and data sample

ALICE is a general purpose heavy-ion experiment. A detailed description of the experimental apparatus can be found in [21]. It consists of a central barrel covering the pseudo-rapidity interval $|\eta| < 0.9$ and a muon spectrometer covering $-4 < \eta < -2.5$.[1] J/ψ production is measured in both rapidity ranges: at mid-rapidity in the dielectron decay channel and at forward-rapidity in the dimuon decay channel. In both cases the J/ψ transverse momentum (p_T) coverage extends down to zero.

At mid-rapidity, the detectors used for the J/ψ analysis are the Inner Tracking System (ITS) [22] and the Time Projection Chamber (TPC) [23]. The ITS is composed of six concentric cylindrical layers of silicon detectors with radii ranging from 3.9 to 43 cm with respect to the beam axis. Its main purpose is to provide the reconstruction of the primary interaction vertex as well as secondary decay vertices of heavy flavored particles. In addition, the two innermost layers can provide an input at level zero (L0) to the trigger system. The TPC, with an active volume extending from 85 to 247 cm in the radial direction, is the main tracking detector of the central barrel and also provides particle identification via the measurement of the specific energy loss (dE/dx) in the detector gas.

At forward-rapidity, the J/ψ analysis is carried out using the muon spectrometer [24]. The spectrometer consists of a ten interaction length front absorber, filtering the muons in front of five tracking stations made of two planes of cathode pad chambers each. The third station is located inside a dipole magnet with a 3 Tm field integral. The spectrometer is completed by a Muon Trigger system (MTR) made of two stations, each equipped with two planes of resistive plate chambers. The trigger chambers are placed behind a 1.2 m thick iron wall to stop secondary hadrons escaping from the front absorber and low momentum muons coming mainly from π and K decays. Throughout its full length, a conical absorber made of tungsten, lead and steel protects the muon spectrometer against secondary particles generated by the interaction with the beam pipe of primary particles produced at large η.

Additional forward detectors, the VZERO [25] and the Zero Degree Calorimeters (ZDC) [26], are used for triggering and event characterization. The VZERO detector is composed of two scintillator arrays, 32 channels each, placed on both sides of the Interaction Point (IP). It covers $2.8 \leq \eta \leq 5.1$ (VZERO-A) and $-3.7 \leq \eta \leq -1.7$ (VZERO-C). The ZDC are located at a distance of 114 m on both sides of the IP and can detect spectator neutrons and protons.

The results presented in this Letter are based on data collected during the 2010 and 2011 LHC Pb–Pb runs for the dielectron analysis and on data collected in the 2011 run for the dimuon one. Forward-rapidity results in the dimuon channel from the 2010 data set, based on an integrated luminosity about 25 times smaller than the 2011 data set, have been published previously in [11]. The minimum bias (MB) trigger for the 2011 data set is defined by the coincidence of signals in the two VZERO arrays synchronized with the passage of two crossing Pb bunches. In the 2010 data set, the MB trigger had an additional requirement on hits in the ITS. The two MB trigger definitions, however, lead to very similar trigger efficiencies, which are larger than 95% for inelastic Pb–Pb collisions. Electromagnetic interactions are rejected at the level one trigger (L1) by applying a cut on the minimum energy deposited by spectator neutrons in the ZDC. Beam induced background is further reduced at the offline level by applying timing cuts on the signals from the VZERO and ZDC detectors.

At mid-rapidity, the 2010 data sample used in the electron analysis consists of 15 million events collected with the MB trigger, corresponding to an integrated luminosity of 2.1 μb^{-1}. The 2011 event sample was enriched with central and semi-central Pb–Pb collisions by using thresholds on the VZERO multiplicity at the L0 trigger. The inspected integrated luminosity amounts to 25.6 μb^{-1}, out of which we analyzed 20 million central (0%–10% of the centrality distribution) and 20 million semi-central (10%–50%) events. The summed 2010 and 2011 datasets correspond to an integrated luminosity of $\mathcal{L}_{int} = 27.7 \pm 0.4(\text{stat.})^{+2.2}_{-1.8}(\text{syst. } \sigma_{\text{Pb–Pb}})$ μb^{-1}. At forward-rapidity, the 2011 data sample is made of about 17 million $\mu\mu$MB triggers. The $\mu\mu$MB trigger is defined as the occurrence of the MB condition in coincidence with the detection in the MTR of two opposite-sign muons tracks. The MTR is capable of (i) delivering L0 trigger decisions at 40 MHz based on the detection of one or two muon trigger tracks, (ii) computing an approximate value of the transverse momentum of muon trigger tracks (p_T^{trig}) and (iii) applying a threshold[2] on the p_T^{trig}. A 1 GeV/c threshold, applied on both muons, was chosen to collect this data sample. A scaling factor F_{norm} is used to obtain the number of equivalent MB events from the number of $\mu\mu$MB ones. It is defined as the ratio, in a MB data sample, of the number of MB events divided by the number of events fulfilling the $\mu\mu$MB trigger condition. Its value, averaged over the entire data sample, is $F_{norm} = 30.56 \pm 0.01(\text{stat.}) \pm 1.10(\text{syst.})$. The integrated luminosity used in this analysis is therefore $\mathcal{L}_{int} = N_{\mu\mu\text{MB}} \times F_{norm}/\sigma_{\text{Pb–Pb}} = 68.8 \pm 0.9(\text{stat.}) \pm 2.5(\text{syst. } F_{norm})^{+5.5}_{-4.5}(\text{syst. } \sigma_{\text{Pb–Pb}})$ μb^{-1} assuming an inelastic Pb–Pb cross-section $\sigma_{\text{Pb–Pb}} = 7.7 \pm 0.1^{+0.6}_{-0.5}$ b [26].

The centrality determination is based on a fit to the VZERO amplitude distribution as described in [27]. The fit, based on the Glauber model, allows for the extraction of collision-related variables such as the average of number of participant nucleons $\langle N_{part} \rangle$ and the average of the nuclear overlap function $\langle T_{AA} \rangle$ per centrality class. Numerical values are given in Table 1. Both the electron and muon analyses were carried out on an event sample corresponding to the most central 90% of the inelastic Pb–Pb cross-section. In this centrality range the efficiency of the MB trigger is 100% and the contamination from electromagnetic processes is negligible.

[1] In the ALICE reference frame, the muon spectrometer covers a negative η range and consequently a negative y range. We have chosen to present our results with a positive y notation.

[2] The threshold is defined as p_T^{trig} for which the trigger probability is 50% and does not lead to a sharp cut in p_T.

Table 1
The average of number of participating nucleons $\langle N_{\rm part}\rangle$ and the average value of the nuclear overlap function $\langle T_{\rm AA}\rangle$ with their associated systematic uncertainty for the centrality classes, expressed in percentages of the nuclear cross-section [27], used in these analyses.

Centrality	$\langle N_{\rm part}\rangle$	$\langle T_{\rm AA}\rangle$ (mb^{-1})
0%–10%	356.0 ± 3.6	23.44 ± 0.76
10%–20%	260.1 ± 3.8	14.39 ± 0.45
20%–30%	185.8 ± 3.3	8.70 ± 0.27
30%–40%	128.5 ± 2.9	5.00 ± 0.18
40%–50%	84.7 ± 2.4	2.68 ± 0.12
50%–60%	52.4 ± 1.6	1.317 ± 0.071
60%–70%	29.77 ± 0.98	0.591 ± 0.036
70%–80%	15.27 ± 0.55	0.243 ± 0.016
80%–90%	7.49 ± 0.22	0.0983 ± 0.0076
0%–20%	308.1 ± 3.7	18.91 ± 0.61
10%–40%	191.5 ± 3.3	9.36 ± 0.30
40%–90%	37.9 ± 1.2	0.985 ± 0.051
0%–90%	124.4 ± 2.2	6.27 ± 0.21

3. Data analysis

J/ψ candidates are formed by combining pairs of opposite-sign (OS) electron and muon tracks reconstructed in the central barrel and in the muon spectrometer, respectively.

Electron candidates are selected by cutting on the quality of tracks reconstructed in the ITS and the TPC. The selection criteria are very similar to those used in the previous analysis of pp collisions at $\sqrt{s} = 7$ TeV [24] using a tighter selection on electron identification. A hit in one of the two innermost layers of the ITS is required. This rejects a large fraction of background resulting from photon conversions in the detector material. The tracks are required to have at least 70 out of a maximum of 159 clusters in the TPC and to pass a quality cut based on the χ^2 of the TPC track fit divided by the number of clusters attached to the track. Electron identification is done using the TPC, requiring the $\mathrm{d}E/\mathrm{d}x$ signal to be compatible with the electron expectation within a band of $(-2.0; +3.0)\sigma$ or $(-1.5; +3.0)\sigma$ for the 2010 or 2011 data, respectively, where σ denotes the resolution of the $\mathrm{d}E/\mathrm{d}x$ measurement. Due to a lower $\mathrm{d}E/\mathrm{d}x$ resolution for the 2011 data, for $|\eta| < 0.5$ a more restrictive electron selection, $(-0.9; +3.0)\sigma$, is applied. The electron/hadron separation is further improved by rejecting tracks which are compatible with the pion expectation within 3.5σ and with the proton expectation within 3.5σ or 4.0σ in 2010 or 2011 data, respectively. Since the electrons from a J/ψ decay have a momentum of 1.5 GeV/c in the mother particle rest frame, a cut of $p_{\rm T} > 0.85$ GeV/c on the candidate tracks is applied to reject the combinatorial background from low momentum electrons. Finally, to ensure good tracking and particle identification in the TPC, only candidates within $|\eta| < 0.8$ are selected.

Muon tracks are reconstructed in the muon spectrometer as detailed in [24] for pp collisions. This procedure remains basically unchanged for Pb–Pb collisions. However, to cope with the large background in central events, some selection criteria were tightened compared to the pp analysis. The search area for finding clusters associated to tracks is reduced by a factor of nine, both muon candidates have to match a track segment in the trigger chambers and the track pseudo-rapidity has to be in the range $-4 < \eta < -2.5$. A further cut on the track transverse coordinate at the end of the front absorber ($R_{\rm abs}$) is applied ($17.6 \leq R_{\rm abs} \leq 89.5$ cm) to ensure that muons emitted at small angles, i.e. those that have crossed a significant fraction of the thick beam shield, are rejected. Finally, to remove events very close to the edge of the spectrometer acceptance, only muon pairs in the rapidity range $2.5 < y < 4$ are accepted.

In the e^+e^- decay channel, the J/ψ yields are extracted by counting the number of entries in the invariant mass range $2.92 < \mathrm{m}_{e^+e^-} < 3.16$ GeV/c^2 after subtracting the combinatorial background. Due to the radiative decay channel and the energy loss of the electrons in the detector material via bremsstrahlung, only $\approx 68\%$ of the J/ψ are reconstructed with the mass in the counting mass interval. The background shape is obtained using the mixed-event (ME) technique. Uncorrelated lepton pairs are created from different Pb–Pb events that have similar global properties such as centrality, primary vertex position and event plane angle. The background shape from ME is scaled to match the same-event (SE) invariant mass distribution in the ranges $1.5 < \mathrm{m}_{e^+e^-} < 2.5$ GeV/c^2 and $3.2 < \mathrm{m}_{e^+e^-} < 4.2$ GeV/c^2. These mass ranges were chosen such that they are close to the signal region and have equal number of bins on each side of the signal region. The lower (1.5 GeV/c^2) and upper (2.5 GeV/c^2) limits of the first mass range are chosen in order to avoid sensitivity to correlated low-mass dielectron pairs and J/ψ bremsstrahlung tail, respectively. The second mass range is limited by the upper limit of the signal region (3.2 GeV/c^2) and extends to 4.2 GeV/c^2 to match in size the first mass interval. Here the influence of the $\psi(2S)$ on the background matching procedure is neglected since the $\psi(2S)$ dilepton yields are expected to be roughly 60 times smaller than J/ψ yields (estimation based on LHCb measurements of J/ψ [28] and $\psi(2S)$ [29] cross-sections in pp collisions at 7 TeV). A good matching between the SE and ME distributions is observed over a broad mass range outside the J/ψ mass region, as visible in the top panels of Fig. 1. This is a clear sign that the contribution of correlated pairs to the OS mass spectrum is small with respect to the uncorrelated background or has a similar shape. The bottom panels of Fig. 1 show the background-subtracted invariant mass spectra compared to the J/ψ signal shape from a Monte-Carlo (MC) simulation. The bremsstrahlung tail from the electron energy loss in the detector material and the J/ψ radiative decay channel ($J/\psi \rightarrow e^+e^-\gamma$) is well described in the MC. As shown in Fig. 1, it is possible to study the J/ψ production in three centrality intervals (0%–10%, 10%–40%, 40%–90%), with a signal-to-background ratio (S/B), evaluated in the range $2.92 < \mathrm{m}_{e^+e^-} < 3.16$ GeV/c^2, increasing from 0.02 to 0.25 from central to peripheral collisions.

In the $\mu^+\mu^-$ decay channel, the J/ψ raw yield is extracted in each centrality and kinematic interval by using two different methods. In the first approach, the OS dimuon invariant mass distribution is fitted with the sum of an extended Crystal Ball (CB2) function to describe the signal, and a Variable Width Gaussian (VWG) function for the background. The CB2 function extends the standard Crystal Ball (Gaussian plus power-law tail at low masses [30]) by an additional power-law tail at high masses with parameters independent of the low mass ones. The VWG function is a Gaussian function with a fourth parameter to allow linear variation of the width with the invariant mass of the dimuon pair. The J/ψ signal is clearly visible in all centrality, $p_{\rm T}$ or y intervals even before any background subtraction, as can be observed in the top panels of Fig. 2, where examples of invariant mass spectra fits in selected $p_{\rm T}$ intervals are shown. The signal-to-background ratio, evaluated within 3 standard deviations with respect to the J/ψ pole mass, varies from 0.16 at low $p_{\rm T}$ up to 1.2 at high $p_{\rm T}$. The corresponding values in centrality and y intervals are in the range 0.16–6.5 from central to peripheral collisions and 0.19–0.59 from low to high rapidity. In all cases, the significance is larger than 10. In the second approach, the combinatorial background was subtracted using an event-mixing technique. The background shape obtained from ME was normalized to the data through a combination of the measured like-sign muon pairs from SE. Fig. 2 (bottom panels) shows the resulting mass distribution fitted with the sum of a CB2 and an exponential which accounts for resid-

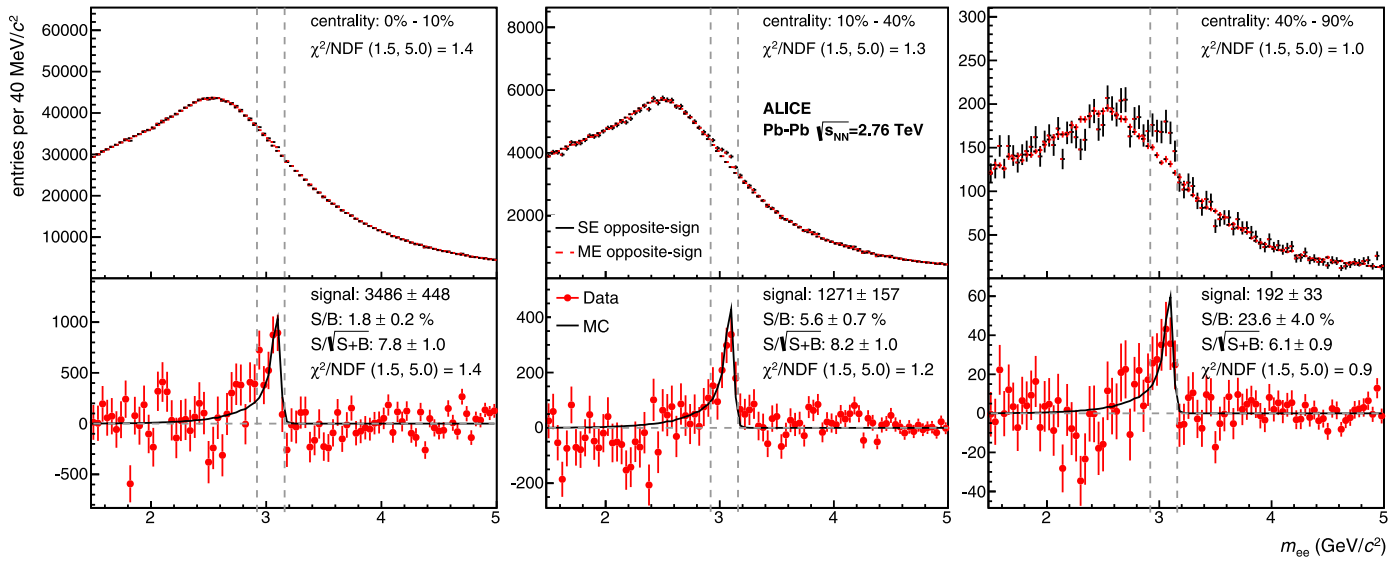

Fig. 1. (Color online.) Top panels: invariant mass distributions for opposite-sign (OS) and mixed-events (ME) electron pairs. Bottom panels: OS invariant mass spectra, after the subtraction of the ME distributions, with a comparison to the Monte Carlo signal (solid lines) superimposed. The MC signal is scaled to match the integral of the OS distribution within the mass counting window. From left to right, distributions correspond to the centrality ranges 0%–10%, 10%–40% and 40%–90%, respectively. The panels for the 0%–10% and 10%–40% centrality ranges are obtained from the 2011 data, while the ones for the 40%–90% centrality range are obtained from the 2010 data. The two vertical dashed lines shown in each panel indicate the mass interval used for signal counting.

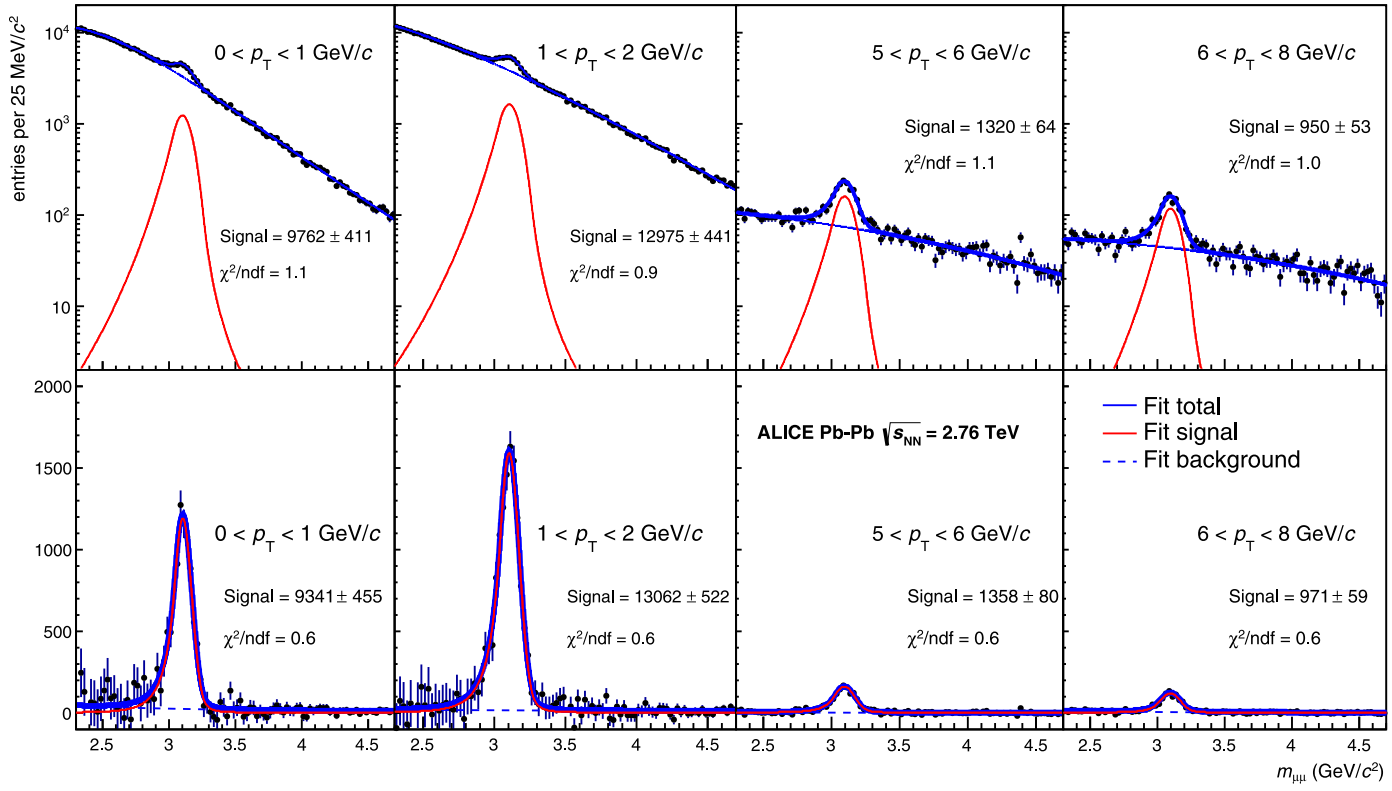

Fig. 2. (Color online.) Top panels: fits of the dimuon invariant mass spectra in selected p_T intervals. Bottom panels: idem after subtraction of the combinatorial background with the event mixing technique. Distributions correspond to the centrality class 0%–90% and $2.5 < y < 4$.

ual correlated background. In both approaches, the position of the peak of the CB2 function ($m_{J/\psi}$), as well as its width ($\sigma_{J/\psi}$), are free parameters of the fit. Their values, obtained by fitting the invariant mass spectrum integrated over p_T, y and centrality, are $m_{J/\psi} = 3.103 \pm 0.001$ GeV/c^2 (shifted up by 0.2% with respect to the PDG mass [31]) and $\sigma_{J/\psi} = 0.071 \pm 0.001$ GeV/c^2. More details about the fitting procedures and the different parameters of the signal and background line shapes are discussed in Section 4.

The measured number of J/ψ ($N^i_{J/\psi}$) in a centrality class i is normalized to the corresponding number of MB events falling in the centrality class (N^i_{events}) and further corrected for the branching ratio (BR) of the dilepton decay channel, the acceptance A and

Table 2
Inclusive J/ψ production cross-sections at mid-rapidity used in the interpolation procedure. The J/ψ are assumed unpolarized and the systematic uncertainties do not include the contribution from unknown polarization.

Experiment	Collision energy $\sqrt{s}$ (TeV)	Rapidity range	$B_{ll}\mathrm{d}\sigma/\mathrm{d}y$ at $y=0$ (nb)	stat. (nb)	syst. (nb)	Reference
PHENIX	0.2	$\lvert y\rvert < 0.35$	44.30	1.40	6.80	[38]
CDF	1.96	$\lvert y\rvert < 0.6$	201.6	1.0	$^{17.8}_{-16.3}$	[39]
ALICE	2.76	$\lvert y\rvert < 0.9$	255.8	58.7	45.9	[40]
ALICE	7	$\lvert y\rvert < 0.9$	409.9	36.8	59.4	[24,41]
Interpolation	2.76	$\lvert y\rvert < 0.8$	252.6	16.4	25.8	this work

the efficiency ϵ^i of the detector. In the $\mu^+\mu^-$ analysis, N^i_{events} is computed by multiplying the number of $\mu\mu$MB triggered events by the F_{norm} factor (described in Section 2) scaled by the width of the centrality class i. The inclusive J/ψ yield for the measured p_{T} and y ranges is then given by:

$$Y^i_{\mathrm{J}/\psi} = \frac{N^i_{\mathrm{J}/\psi}}{\mathrm{BR}_{\mathrm{J}/\psi\to l^+l^-} N^i_{\mathrm{events}} A\times\epsilon^i}. \quad (1)$$

The acceptance times efficiency product ($A\times\varepsilon$) is defined as the ratio between the number of reconstructed J/ψ divided by the number of generated ones in the kinematic range under study. In the e^+e^- decay channel, $A\times\varepsilon$ is calculated from MC simulations. These MC events are a superposition of Pb–Pb collisions generated with an appropriate HIJING [32] tune reproducing the measured charged particle density [33] and J/ψ generated from parametrized p_{T} and y distributions (details in Section 4). The J/ψ dielectron decays are performed using PHOTOS [34,35]. The particles are then transported through a simulation of the ALICE detector using GEANT 3.21 [36]. The geometrical acceptance is about 34%. The estimated integrated $A\times\varepsilon$ for the J/ψ emitted in $\lvert y\rvert < 0.8$ amount to 0.080, 0.085 and 0.093 for the 0%–10%, 10%–40% and 40%–90% centrality classes in the 2010 data sample and 0.026 and 0.028 for the 0%–10% and 10%–40% centrality classes in the 2011 one, respectively. The large difference in efficiency is mainly due to a lower efficiency of the two innermost ITS layers and stronger particle identification cuts used for the 2011 data set. In the $\mu^+\mu^-$ decay channel, $A\times\varepsilon$ was computed using an embedding technique where MC J/ψ particles are injected into the raw data of real events and then reconstructed. The MC J/ψ p_{T} and y parametrization is taken from actual measurements. PYTHIA [37] takes care of the J/ψ decays and the daughter particles signals in the detector, given by GEANT 3.21, are then added to the real Pb–Pb events. When studied as a function of centrality, $A\times\varepsilon$ decreases by 7.9%, from 0.127 in the 80%–90% centrality class to 0.117 in the 0%–10% one. The centrality integrated $A\times\varepsilon$ (0%–90% centrality class) is 0.120 with a negligible statistical uncertainty. The geometrical acceptance is about 18%. The quantity $A\times\varepsilon$ shows a non-monotonic dependence on p_{T}, starting at approximately 0.124 at zero transverse momentum, reaching a minimum of 0.103 at 1.5 GeV/c and then linearly increasing up to 0.264 at 8 GeV/c. The rapidity dependence of $A\times\varepsilon$ reflects the geometrical acceptance of the muon pairs with a maximum of 0.189 centered at $y=3.3$ decreasing towards the edges of the acceptance to 0.033 (0.060) at $y=2.5$ ($y=4.0$).

Finally, the nuclear modification factor is calculated as the ratio between the corrected J/ψ yield in Pb–Pb collisions $Y^{\mathrm{Pb-Pb}}_{\mathrm{J}/\psi}$ and the J/ψ cross-section in pp collisions scaled by the nuclear overlap function:

$$R_{\mathrm{AA}} = \frac{Y^{\mathrm{Pb-Pb}}_{\mathrm{J}/\psi}}{\langle T_{\mathrm{AA}}\rangle\times\sigma^{\mathrm{pp}}_{\mathrm{J}/\psi}}. \quad (2)$$

In the dielectron analysis, the pp reference was obtained by interpolating the inclusive J/ψ cross-sections at mid-rapidity measured by PHENIX [8] at $\sqrt{s}=0.2$ TeV, CDF [39] at $\sqrt{s}=1.96$ TeV and ALICE [40,24,41] at $\sqrt{s}=2.76$ and 7 TeV. All the data points used in this procedure are listed in Table 2. The interpolation was done by fitting the data points with several functions assuming a linear, an exponential, a power law or a polynomial $\sqrt{s}$ dependence. The value of the interpolated pp reference at mid-rapidity, $\mathrm{d}\sigma^{\mathrm{pp}}_{\mathrm{J}/\psi}/\mathrm{d}y = 4.25\pm0.28(\mathrm{stat.})\pm0.43(\mathrm{syst.})$ μb, is consistent with the one measured by ALICE [40], but the total uncertainty is twice smaller, being driven mainly by the CDF result. The statistical uncertainty was obtained from the fitting procedure, while the systematic one was obtained by changing the fit function and by shifting the data points within their experimental systematic uncertainties. For the dimuon analysis, the pp reference and its associated uncertainties are extracted from the ALICE measurement [40].

4. Systematic uncertainties

The main sources of systematic uncertainties for the J/ψ R_{AA} evaluation are the tracking efficiency, the signal extraction procedure, the parameterization of the J/ψ kinematic distributions used as input for the MC simulations, the uncertainty on the nuclear overlap function and the uncertainty on the J/ψ pp cross-section at $\sqrt{s}=2.76$ TeV. Other analysis-dependent sources are detailed in the following. The systematic uncertainties have been evaluated as a function of centrality and, for the dimuon analysis, of p_{T} and y. An overview of systematic uncertainties is given in Table 3.

In the dielectron analysis, the systematic uncertainties on the signal extraction are estimated by varying the mass region used to count the signal, the mass interval used for matching the ME background and the OS distribution. In all these cases, the background-subtracted OS distribution is compared to the MC signal shape and the normalized χ^2 obtained is always close to 1. This shows that, after background subtraction, the number of correlated pairs not related to J/ψ decays is small and does not induce a sizeable systematic uncertainty. The centrality dependent systematic uncertainty on the signal extraction, taken as the RMS of the distribution of the number of J/ψ obtained from all the performed tests, ranges from 7% to 9% and 4% to 6% for 2010 and 2011 data, respectively. The systematic uncertainties due to track reconstruction and particle identification are evaluated by varying all the analysis cuts. For each cut variation, the number of J/ψ signal counts is corrected with the corresponding $A\times\varepsilon$. The RMS of this quantity is found to vary in the range 6–9% and 4–5% in the 2010 and 2011 data, respectively. Since the signal extraction procedure must be used for every cut variation, the systematic uncertainties due to analysis cuts and signal extraction cannot be truly disentangled. Thus, a global systematic uncertainty is introduced as the RMS of the distribution of corrected results when varying both signal extraction parameters and cut values. These systematic uncertainties range between 8% and 11% depending on the centrality interval. The central value for the corrected J/ψ yield is chosen to be the mean of the distribution obtained from all the performed tests.

In the dimuon analysis, the systematic uncertainty on the signal extraction is estimated by fitting the invariant mass distribution

Table 3
Systematic uncertainties entering the R_{AA} calculation. The type I (II) stands for correlated (uncorrelated) uncertainties within a given set of data points. The uncorrelated systematic uncertainties (type II) are given as a range.

Channel	$\mu^+\mu^-$				e^+e^-	
	Centrality		p_T or y		Centrality	
	value (%)	type	value (%)	type	value (%)	type
signal extraction	1–3	II	1–5	II	8–11	II
tracking efficiency	11 and 0–1	I and II	1 and 8–14	I and II		
trigger efficiency	2 and 0–1	I and II	1 and 2–4	I and II	n/a	
input MC parameterization	3	I	0–8	II	5	I
matching efficiency	1	I	1	II	n/a	
centrality limits	0–5	II	0–1	I	0–3	II
$\langle T_{AA}\rangle$	3–8	II	3	I	3–5	II
$\sigma^{pp}_{J/\psi}$	9	I	6 and 5–6	I and II	12	I
F_{norm}	4	I	4	I	n/a	

with and without background subtraction and by varying the parameters that define the power law shapes at low and high masses of the CB2 signal function. These fit parameters are not constrained by the data and cannot be let free during the fitting procedure. They have been fixed to different values extracted either from simulations or from pp data, where the signal-to-background ratio is more favorable. Fits corresponding to the various choices for the CB2 tails are performed, keeping the background parameters free, and varying the invariant mass range used for the fits. The raw J/ψ yield is determined as the average of the results obtained with the above procedure and the corresponding systematic uncertainty is defined as the RMS of the deviations from the average. As a function of centrality (p_T or y) the systematic uncertainty for the signal extraction varies from 1% to 3% (1% to 5%). The single muon tracking and trigger efficiencies, ϵ_{trk} and ϵ_{trg}, are estimated with the embedded J/ψ simulation. The centrality dependence of these quantities is weak, since the decrease in most central collisions is about 1% and 3.5% for ϵ_{trk} and ϵ_{trg} respectively. A 11% systematic uncertainty on the tracking efficiency is estimated by comparing its determination based on real data and on a MC approach. This estimation relies on a calculation of the tracking efficiency in each station using the detector redundancy (two independent detection planes per station). The single track efficiency, defined as product of the station efficiencies, is calculated for tracks from real data and from simulation. The single track efficiencies are then injected in pure J/ψ simulations and the difference used as the J/ψ tracking systematic uncertainty. The p_T and y dependence of the former uncertainty leads to a bin to bin uncorrelated component ranging between 8% and 14%. The systematic uncertainty on the J/ψ $A\times\varepsilon$ corrections related to the trigger efficiency is 2%, mostly given by the uncertainty on the intrinsic efficiency of the trigger chambers. The systematic uncertainty related to the response function of the trigger is always below 1% except in the lowest J/ψ p_T interval where a value of 3% was estimated. As a function of centrality, the systematic uncertainty of the tracking or the trigger efficiencies is 1% in the most central collisions and becomes negligible for peripheral collisions. The uncertainty on the matching efficiency between tracks reconstructed in the tracking and trigger chambers amounts to 1%. It is correlated as a function of the centrality and uncorrelated as a function of p_T and y.

The $A\times\varepsilon$ calculation depends on the J/ψ p_T and y distributions used as an input to the MC, and systematic effects originating from different parameterizations of these distributions must be taken into account. In the e^+e^- analysis, the J/ψ (p_T, y) parameterization is based on an interpolation of the RHIC, CDF and LHC data in pp and $p\bar{p}$ collisions [42] corrected using nuclear shadowing calculations [43]. The systematic uncertainty was evaluated by varying the slope of the p_T shape in a wide range such that the average p_T changes between 1.5 GeV/c and 3.0 GeV/c. The J/ψ p_T spectra in A–A collisions measured by PHENIX [9] at mid-rapidity and ALICE at forward rapidity [40] at all available centralities, together with their uncertainties, are well covered in the envelope determined by the considered variations. A centrality correlated systematic uncertainty of 5% was obtained following this procedure. In the $\mu^+\mu^-$ analysis, the MC J/ψ parameterizations are based on the p_T and y distributions measured for different centrality classes. The p_T–y correlation observed by LHCb in pp collisions [28] was also included in the systematic study. A correlated variation in $A\times\varepsilon$ of 3% was observed as a function of centrality. The p_T (y) dependence of this systematic uncertainty brings a maximum contribution of 1% (8%) on each point.

Further sources of systematic uncertainties affecting the nuclear modification factor are the uncertainty on the limits of the centrality classes [27], on the nuclear overlap function and on the J/ψ cross-section in pp collisions at $\sqrt{s}=2.76$ TeV. An uncertainty on the normalization factor F_{norm}, accounting for run by run fluctuations on this quantity, is also added in the muon analysis. All numerical values can be found in Table 3.

When computing the $A\times\varepsilon$ factor, we assumed that J/ψ are produced unpolarized and no systematic uncertainty is assigned to a possible polarization. In pp collisions, mid-rapidity ($p_T>10$ GeV/c) and forward-rapidity ($p_T>2$ GeV/c) measurements have been done at $\sqrt{s}=7$ TeV and indeed show that J/ψ polarization is compatible with zero [44–46]. In Pb–Pb collisions, J/ψ mesons produced from charm quarks in the medium are expected to be unpolarized.

5. Results

In the e^+e^- decay channel, the inclusive J/ψ R_{AA} was studied as a function of the collision centrality (0%–10%, 10%–40% and 40%–90%) for $p_T>0$ GeV/c and $|y|<0.8$. In the $\mu^+\mu^-$ decay channel, the event sample collected in the 2011 run with the dedicated $\mu\mu$MB trigger allows for the study of the R_{AA} as a function of the centrality of the collisions in nine intervals. Furthermore, a differential study of the R_{AA} as a function of transverse momentum or rapidity is also feasible. Data are analyzed in seven intervals in the p_T range $0<p_T<8$ GeV/c range and six intervals in the y range $2.5<y<4$. The chosen binning matches the one adopted for the $\sqrt{s}=2.76$ TeV pp results, which are used as the reference for the evaluation of the nuclear modification factor.

Fig. 3 shows the inclusive J/ψ R_{AA} at mid- and forward-rapidity as a function of the number of participant nucleons $\langle N_{part}\rangle$. Statistical uncertainties are shown as vertical error bars, while the boxes represent the various uncorrelated systematic uncertainties added in quadrature. The systematic uncertainties correlated bin by bin (type II in Table 3) are summed in quadrature and referred to as *global syst.* in the legend. At forward-rapidity a clear suppression

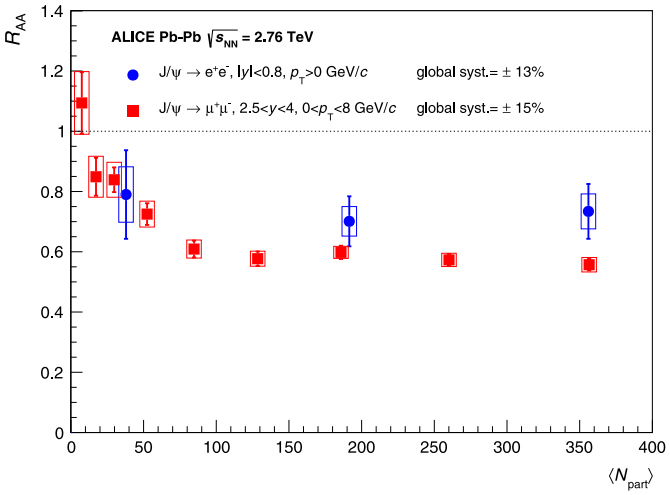

Fig. 3. (Color online.) Centrality dependence of the nuclear modification factor, R_{AA}, of inclusive J/ψ production in Pb–Pb collisions at $\sqrt{s_{NN}} = 2.76$ TeV, measured at mid-rapidity and at forward-rapidity. The point to point uncorrelated systematic uncertainties (type II) are represented as boxes around the data points, while the statistical ones are shown as vertical bars. Global correlated systematic uncertainties (type I) are quoted directly in the legend.

is observed, independent of centrality for $\langle N_{\rm part}\rangle > 70$. Although with larger uncertainties, the mid-rapidity R_{AA} shows a suppression of the J/ψ yield too. The centrality integrated R_{AA} values are $R_{AA}^{0\%-90\%} = 0.72 \pm 0.06(\text{stat.}) \pm 0.10(\text{syst.})$ and $R_{AA}^{0\%-90\%} = 0.58 \pm 0.01(\text{stat.}) \pm 0.09(\text{syst.})$ at mid- and forward-rapidity, respectively. The systematic uncertainties on both R_{AA} values include the contribution arising from $\langle T_{AA}\rangle$ calculations. This amounts to 3.4% of the computed $\langle T_{AA}\rangle$ value and is a correlated systematic uncertainty common to the mid- and forward-rapidity measurements. PHENIX mid- ($|y| < 0.35$) and forward-rapidity ($1.2 < |y| < 2.2$) results on inclusive J/ψ R_{AA} at $\sqrt{s_{NN}} = 0.2$ TeV exhibit a much stronger dependence on the collision centrality and a suppression of about a factor of three larger in the most central collisions [9].

The measured inclusive J/ψ R_{AA} includes contributions from prompt and non-prompt J/ψ; the first one results from direct J/ψ production and feed-down from ψ(2S) and χ_c, the second one arises from beauty hadron decays. Non-prompt J/ψ are different with respect to the prompt ones, since their suppression or production is insensitive to color screening or regeneration mechanisms. Beauty hadron decay mostly occurs outside the fireball, and a measurement of the non-prompt J/ψ R_{AA} is therefore connected to the beauty quark in-medium energy loss (see [47] and references therein). At mid-rapidity, the contribution from beauty hadron feed-down to the inclusive J/ψ yield in pp collisions at $\sqrt{s} = 7$ TeV is approximately 15% [48]. The prompt J/ψ R_{AA} can be evaluated according to $R_{AA}^{prompt} = (R_{AA} - R_{AA}^{non\text{-}prompt})/(1 - F_B)$ where F_B is the fraction of non-prompt J/ψ measured in pp collisions, and $R_{AA}^{non\text{-}prompt}$ is the nuclear modification factor of beauty hadrons in Pb–Pb collisions. Thus, the prompt J/ψ R_{AA} at mid-rapidity is expected to be about 7% smaller than the inclusive measurement if the beauty production scales with the number of binary collisions ($R_{AA}^{non\text{-}prompt} = 1$) and about 17% larger if the beauty is fully suppressed ($R_{AA}^{non\text{-}prompt} = 0$). At forward-rapidity, the non-prompt J/ψ fraction was measured by the LHCb Collaboration to be about 11(7)% in pp collisions at $\sqrt{s} = 7(2.76)$ TeV in the p_T range covered by this analysis [28,49]. Then, the difference between the R_{AA} of prompt J/ψ and the one for inclusive J/ψ is expected to be of about −6% and 7% in the two aforementioned extreme cases assumed for beauty production.

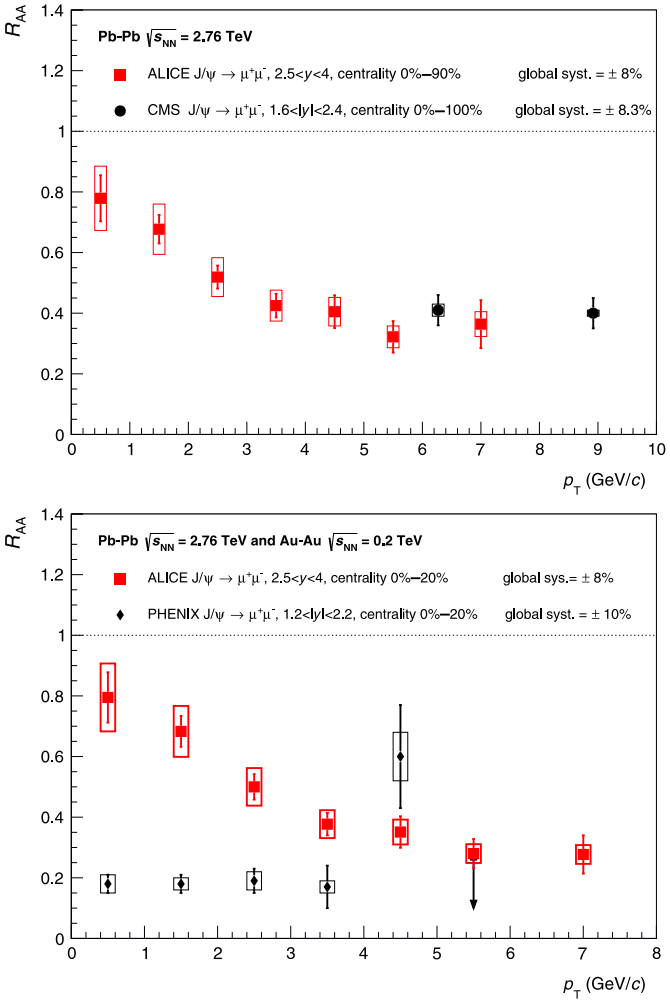

Fig. 4. (Color online.) Top panel: transverse momentum dependence of the centrality integrated J/ψ R_{AA} measured by ALICE in Pb–Pb collisions at $\sqrt{s_{NN}} = 2.76$ TeV compared to CMS [20] results at the same $\sqrt{s_{NN}}$. Bottom panel: transverse momentum dependence of the J/ψ R_{AA} measured by ALICE in the 0%–20% most central Pb–Pb collisions at $\sqrt{s_{NN}} = 2.76$ TeV compared to PHENIX [9] results in the 0%–20% most central Au–Au collisions at $\sqrt{s_{NN}} = 0.2$ TeV.

In the top panel of Fig. 4, the J/ψ R_{AA} at forward-rapidity is shown as a function of p_T for the 0%–90% centrality integrated Pb–Pb collisions. It exhibits a decrease from 0.78 to 0.36, indicating that high p_T J/ψ are more suppressed than low p_T ones. Furthermore, at high p_T a direct comparison with CMS results [20] at the same $\sqrt{s_{NN}}$ is possible, the main difference being that the CMS measurement covers a slightly more central rapidity range ($1.6 < |y| < 2.4$). In the overlapping p_T range a similar suppression is found. One should add here that the two CMS points are not independent and correspond to different intervals of the J/ψ p_T ($3 < p_T < 30$ GeV/c and $6.5 < p_T < 30$ GeV/c). In the bottom panel of Fig. 4, the forward-rapidity J/ψ R_{AA} for the 0%–20% most central collisions is shown. The observed p_T dependence of the R_{AA} for most central collisions is very close to the one in the 0%–90% centrality class. This is indeed expected since almost 70% of the J/ψ yield is contained in the 0%–20% centrality class. Our data are compared to results obtained by PHENIX in 0%–20% most central Au–Au collisions at $\sqrt{s_{NN}} = 0.2$ TeV, in the rapidity region $1.2 < |y| < 2.2$ [9]. A striking difference between the J/ψ R_{AA} patterns can be observed. In particular, in the low p_T region the ALICE R_{AA} result is a factor of up to four higher compared to the PHENIX one. This observation is in qualitative agreement with the

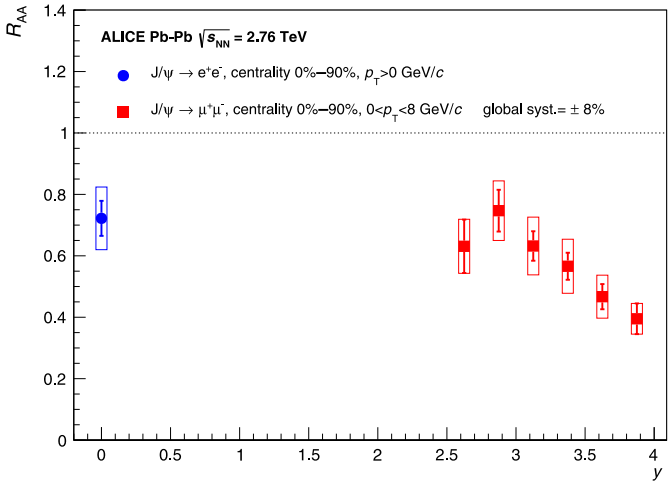

Fig. 5. (Color online.) The rapidity dependence of the J/ψ R_{AA} measured in Pb–Pb collisions at $\sqrt{s_{NN}} = 2.76$ TeV. Both mid- and forward-rapidity measurements include a common correlated systematic uncertainty of 3.4% due to $\langle T_{AA} \rangle$. The mid-rapidity measurement covers the rapidity range $|y| < 0.8$ and the forward-rapidity one is given in intervals of 0.25 unit of rapidity from $y = 2.5$ to $y = 4$.

calculations from [17,50] where the (re)combination dominance in the J/ψ production leads to a decrease of the $\langle p_T^2 \rangle$ in A–A collisions with respect to pp collisions. Although at the two energies the rapidity coverages are not the same and CNM effects might have a different size, our results point to the presence of a new contribution to the J/ψ yield at low p_T.

Finally, the dependence of the J/ψ R_{AA} on rapidity is displayed in Fig. 5 for the 0%–90% centrality class. At forward-rapidity, the J/ψ R_{AA} decreases by about 40% from $y = 2.5$ to $y = 4$. The result from the electron analysis is consistent with a constant or slightly increasing R_{AA} towards mid-rapidity.

6. Conclusions

The inclusive J/ψ nuclear modification factor has been measured by ALICE as a function of centrality, p_T and y in Pb–Pb collisions at $\sqrt{s_{NN}} = 2.76$ TeV, down to zero p_T. At forward-rapidity, R_{AA} shows a clear suppression of the J/ψ yield, with no significant dependence on centrality for $\langle N_{part} \rangle$ larger than 70. At mid-rapidity, the J/ψ R_{AA} is compatible with a constant suppression as a function of centrality. At forward-rapidity the J/ψ R_{AA} exhibits a strong p_T dependence and decreases by a factor of 2 from low p_T to high p_T. This behavior strongly differs from that observed by PHENIX at $\sqrt{s_{NN}} = 0.2$ TeV. This result suggests that a fraction of the J/ψ yield is produced via (re)combination of charm quarks. In addition, the indication of a non-zero J/ψ elliptic flow in Pb–Pb collisions at $\sqrt{s_{NN}} = 2.76$ TeV observed by ALICE [51] brings another hint in favor of (re)combination scenarios. Precise knowledge of the cold nuclear effects is necessary for further understanding of the J/ψ behavior. The measurement of the J/ψ production in p–Pb collisions at the LHC [52,53] will allow one to sharpen the interpretation of these results.

Acknowledgements

The ALICE Collaboration would like to thank all its engineers and technicians for their invaluable contributions to the construction of the experiment and the CERN accelerator teams for the outstanding performance of the LHC complex.

The ALICE Collaboration gratefully acknowledges the resources and support provided by all Grid centres and the Worldwide LHC Computing Grid (WLCG) Collaboration.

The ALICE Collaboration acknowledges the following funding agencies for their support in building and running the ALICE detector: State Committee of Science, World Federation of Scientists (WFS) and Swiss Fonds Kidagan, Armenia; Conselho Nacional de Desenvolvimento Científico e Tecnológico (CNPq), Financiadora de Estudos e Projetos (FINEP), Fundação de Amparo à Pesquisa do Estado de São Paulo (FAPESP); National Natural Science Foundation of China (NSFC), the Chinese Ministry of Education (CMOE) and the Ministry of Science and Technology of China (MSTC); Ministry of Education and Youth of the Czech Republic; Danish Natural Science Research Council, the Carlsberg Foundation and the Danish National Research Foundation; The European Research Council under the European Community's Seventh Framework Programme; Helsinki Institute of Physics and the Academy of Finland; French CNRS-IN2P3, the 'Region Pays de Loire', 'Region Alsace', 'Region Auvergne' and CEA, France; German BMBF and the Helmholtz Association; General Secretariat for Research and Technology, Ministry of Development, Greece; Hungarian OTKA and National Office for Research and Technology (NKTH); Department of Atomic Energy and Department of Science and Technology of the Government of India; Istituto Nazionale di Fisica Nucleare (INFN) and Centro Fermi – Museo Storico della Fisica e Centro Studi e Ricerche "Enrico Fermi", Italy; MEXT Grant-in-Aid for Specially Promoted Research, Japan; Joint Institute for Nuclear Research, Dubna; National Research Foundation of Korea (NRF); CONACYT, DGAPA, México, ALFA-EC and the EPLANET Program (European Particle Physics Latin American Network); Stichting voor Fundamenteel Onderzoek der Materie (FOM) and the Nederlandse Organisatie voor Wetenschappelijk Onderzoek (NWO), Netherlands; Research Council of Norway (NFR); Polish Ministry of Science and Higher Education; National Science Centre, Poland; Ministry of National Education/Institute for Atomic Physics and CNCS-UEFISCDI – Romania; Ministry of Education and Science of Russian Federation, Russian Academy of Sciences, Russian Federal Agency of Atomic Energy, Russian Federal Agency for Science and Innovations and The Russian Foundation for Basic Research; Ministry of Education of Slovakia; Department of Science and Technology, South Africa; CIEMAT, EELA, Ministerio de Economía y Competitividad (MINECO) of Spain, Xunta de Galicia (Consellería de Educación), CEADEN, Cubaenergía, Cuba, and IAEA (International Atomic Energy Agency); Swedish Research Council (VR) and Knut & Alice Wallenberg Foundation (KAW); Ukraine Ministry of Education and Science; United Kingdom Science and Technology Facilities Council (STFC); The United States Department of Energy, the United States National Science Foundation, the State of Texas, and the State of Ohio.

References

[1] T. Matsui, H. Satz, J/ψ suppression by quark–gluon plasma formation, Phys. Lett. B 178 (1986) 416.
[2] F. Karsch, H. Satz, The spectral analysis of strongly interacting matter, Z. Phys. C 51 (1991) 209–224, http://dx.doi.org/10.1007/BF01475790.
[3] S. Digal, P. Petreczky, H. Satz, Quarkonium feed-down and sequential suppression, Phys. Rev. D 64 (2001) 094015, http://dx.doi.org/10.1103/PhysRevD.64.094015.
[4] P. Faccioli, C. Lourenco, J. Seixas, H. Woehri, Study of ψ' and χ_c decays as feed-down sources of J/ψ hadro-production, J. High Energy Phys. 0810 (2008) 004, http://dx.doi.org/10.1088/1126-6708/2008/10/004, arXiv:0809.2153.
[5] B. Alessandro, et al., A new measurement of J/ψ suppression in Pb–Pb collisions at 158 GeV per nucleon, Eur. Phys. J. C 39 (2005) 335–345, http://dx.doi.org/10.1140/epjc/s2004-02107-9, arXiv:hep-ex/0412036.
[6] R. Arnaldi, J/ψ production in p–A and A–A collisions at fixed target experiments, Nucl. Phys. A 830 (2009) 345C–352C, http://dx.doi.org/10.1016/j.nuclphysa.2009.10.030, arXiv:0907.5004.
[7] A. Adare, et al., Cold nuclear matter effects on J/Psi as constrained by deuteron–gold measurements at s(NN)**(1/2) = 200-GeV, Phys. Rev. C 77 (2008) 024912, http://dx.doi.org/10.1103/PhysRevC.79.059901, arXiv:0711.3917.
[8] A. Adare, et al., J/ψ production vs centrality, transverse momentum, and rapidity in Au + Au collisions at $\sqrt{s_{NN}} = 200$ GeV, Phys. Rev. Lett. 98

(2007) 232301, http://dx.doi.org/10.1103/PhysRevLett.98.232301, arXiv:nucl-ex/0611020.
[9] A. Adare, et al., J/ψ suppression at forward rapidity in Au + Au collisions at $\sqrt{s_{NN}} = 200$ GeV, Phys. Rev. C 84 (2011) 054912, http://dx.doi.org/10.1103/PhysRevC.84.054912, arXiv:1103.6269.
[10] S. Chatrchyan, et al., Observation of sequential Upsilon suppression in PbPb collisions, Phys. Rev. Lett. 109 (2012) 222301, http://dx.doi.org/10.1103/PhysRevLett.109.222301, arXiv:1208.2826.
[11] B. Abelev, et al., J/ψ suppression at forward rapidity in Pb–Pb collisions at $\sqrt{s_{NN}} = 2.76$ TeV, Phys. Rev. Lett. 109 (2012) 072301, http://dx.doi.org/10.1103/PhysRevLett.109.072301, arXiv:1202.1383.
[12] B. Abelev, et al., Measurement of charm production at central rapidity in proton–proton collisions at $\sqrt{s} = 2.76$ TeV, J. High Energy Phys. 1207 (2012) 191, http://dx.doi.org/10.1007/JHEP07(2012)191, arXiv:1205.4007.
[13] P. Braun-Munzinger, J. Stachel, (Non)thermal aspects of charmonium production and a new look at J/ψ suppression, Phys. Lett. B 490 (2000) 196–202, http://dx.doi.org/10.1016/S0370-2693(00)00991-6, arXiv:nucl-th/0007059.
[14] R.L. Thews, M. Schroedter, J. Rafelski, Enhanced J/ψ production in deconfined quark matter, Phys. Rev. C 63 (2001) 054905, http://dx.doi.org/10.1103/PhysRevC.63.054905, arXiv:hep-ph/0007323.
[15] M.I. Gorenstein, A. Kostyuk, H. Stöcker, W. Greiner, Statistical coalescence model with exact charm conservation, Phys. Lett. B 509 (2001) 277–282, http://dx.doi.org/10.1016/S0370-2693(01)00516-0, arXiv:hep-ph/0010148.
[16] A. Andronic, P. Braun-Munzinger, K. Redlich, J. Stachel, Evidence for charmonium generation at the phase boundary in ultra-relativistic nuclear collisions, Phys. Lett. B 652 (2007) 259–261, http://dx.doi.org/10.1016/j.physletb.2007.07.036, arXiv:nucl-th/0701079.
[17] X. Zhao, R. Rapp, Transverse momentum spectra of J/ψ in heavy-ion collisions, Phys. Lett. B 664 (2008) 253–257, http://dx.doi.org/10.1016/j.physletb.2008.03.068, arXiv:0712.2407.
[18] Y.-p. Liu, Z. Qu, N. Xu, P.-f. Zhuang, J/ψ transverse momentum distribution in high energy nuclear collisions at RHIC, Phys. Lett. B 678 (2009) 72–76, http://dx.doi.org/10.1016/j.physletb.2009.06.006, arXiv:0901.2757.
[19] G. Aad, et al., Measurement of the centrality dependence of J/ψ yields and observation of Z production in lead–lead collisions with the ATLAS detector at the LHC, Phys. Lett. B 697 (2011) 294–312, http://dx.doi.org/10.1016/j.physletb.2011.02.006, arXiv:1012.5419.
[20] S. Chatrchyan, et al., Suppression of non-prompt J/ψ, prompt J/ψ, and Y(1S) in PbPb collisions at $\sqrt{s_{NN}} = 2.76$ TeV, J. High Energy Phys. 1205 (2012) 063, http://dx.doi.org/10.1007/JHEP05(2012)063, arXiv:1201.5069.
[21] K. Aamodt, et al., The ALICE experiment at the CERN LHC, J. Instrum. 3 (2008) S08002.
[22] ALICE Collaboration, Alignment of the ALICE Inner Tracking System with cosmic-ray tracks, J. Instrum. 5 (2010) 3003, http://dx.doi.org/10.1088/1748-0221/5/03/P03003, arXiv:1001.0502.
[23] J. Alme, et al., The ALICE TPC, a large 3-dimensional tracking device with fast readout for ultra-high multiplicity events, Nucl. Instrum. Methods Phys. Res., Sect. A, Accel. Spectrom. Detect. Assoc. Equip. 622 (2010) 316–367, http://dx.doi.org/10.1016/j.nima.2010.04.042, arXiv:1001.1950.
[24] K. Aamodt, et al., Rapidity and transverse momentum dependence of inclusive J/ψ production in pp collisions at $\sqrt{s} = 7$ TeV, Phys. Lett. B 704 (2011) 442–455, http://dx.doi.org/10.1016/j.physletb.2011.09.054, arXiv:1105.0380.
[25] E. Abbas, et al., Performance of the ALICE VZERO system, J. Instrum. 8 (10) (2013) P10016, arXiv:1306.3130, URL http://stacks.iop.org/1748-0221/8/i=10/a=P10016.
[26] B. Abelev, et al., Measurement of the cross section for electromagnetic dissociation with neutron emission in Pb–Pb collisions at $\sqrt{s_{NN}} = 2.76$ TeV, Phys. Rev. Lett. 109 (2012) 252302, http://dx.doi.org/10.1103/PhysRevLett.109.252302, arXiv:1203.2436.
[27] B. Abelev, et al., Centrality determination of Pb–Pb collisions at sqrt(sNN) = 2.76 TeV with ALICE, Phys. Rev. C 88 (2013) 044909, http://dx.doi.org/10.1103/PhysRevC.88.044909, arXiv:1301.4361.
[28] R. Aaij, et al., Measurement of J/ψ production in pp collisions at $\sqrt{s} = 7$ TeV, Eur. Phys. J. C 71 (2011) 1645, http://dx.doi.org/10.1140/epjc/s10052-011-1645-y, arXiv:1103.0423.
[29] R. Aaij, et al., Measurement of $\psi(2S)$ meson production in pp collisions at sqrt(s) = 7 TeV, Eur. Phys. J. C 72 (2012) 2100, http://dx.doi.org/10.1140/epjc/s10052-012-2100-4, arXiv:1204.1258.
[30] J.E. Gaiser, Charmonium spectroscopy from radiative decays of the J/ψ and ψ', PhD thesis, Standford, appendix-F, SLAC-R-255, 1982.
[31] J. Beringer, et al., Review of particle physics (RPP), Phys. Rev. D 86 (2012) 010001, http://dx.doi.org/10.1103/PhysRevD.86.010001.
[32] X. Wang, M. Gyulassy, HIJING: A Monte Carlo model for multiple jet production in pp, pA and AA collisions, Phys. Rev. D 44 (1991) 3501–3516, http://link.aps.org/doi/10.1103/PhysRevD.44.3501.
[33] K. Aamodt, et al., Centrality dependence of the charged-particle multiplicity density at mid-rapidity in Pb–Pb collisions at $\sqrt{s_{NN}} = 2.76$ TeV, Phys. Rev. Lett. 106 (2011) 032301, http://dx.doi.org/10.1103/PhysRevLett.106.032301, arXiv:1012.1657.
[34] E. Barberio, B. van Eijk, Z. Was, Comput. Phys. Commun. 66 (1991) 115.
[35] E. Barberio, Z. Was, Comput. Phys. Commun. 79 (1994) 291.
[36] R. Brun, et al., GEANT detector description and simulation tool, CERN program library long writeup.
[37] T. Sjostrand, S. Mrenna, P.Z. Skands, PYTHIA 6.4 physics and manual, J. High Energy Phys. 0605 (2006) 026, http://dx.doi.org/10.1088/1126-6708/2006/05/026, arXiv:hep-ph/0603175.
[38] A. Adare, et al., J/ψ production versus transverse momentum and rapidity in p^+p collisions at $\sqrt{s} = 200$-GeV, Phys. Rev. Lett. 98 (2007) 232002, http://dx.doi.org/10.1103/PhysRevLett.98.232002, arXiv:hep-ex/0611020.
[39] D. Acosta, et al., Measurement of the J/ψ meson and b-hadron production cross sections in $p\bar{p}$ collisions at $\sqrt{s} = 1960$ GeV, Phys. Rev. D 71 (2005) 032001, http://dx.doi.org/, arXiv:hep-ex/0412071.
[40] B. Abelev, et al., Inclusive J/ψ production in pp collisions at $\sqrt{s} = 2.76$ TeV, Phys. Lett. B 718 (2012) 295–306, http://dx.doi.org/10.1016/j.physletb.2012.10.078, arXiv:1203.3641.
[41] K. Aamodt, et al., Erratum to "Rapidity and transverse momentum dependence of inclusive production in pp collisions at $\sqrt{s} = 7$ TeV" [Phys. Lett. B 704 (5) (2011) 442], Phys. Lett. B 718 (2) (2012) 692–698, http://dx.doi.org/10.1016/j.physletb.2012.10.060.
[42] F. Bossu, Z.C. del Valle, A. de Falco, M. Gagliardi, S. Grigoryan, et al., Phenomenological interpolation of the inclusive J/ψ cross section to proton–proton collisions at 2.76 TeV and 5.5 TeV, arXiv:1103.2394.
[43] K. Eskola, V. Kolhinen, C. Salgado, The scale dependent nuclear effects in parton distributions for practical applications, Eur. Phys. J. C 9 (1999) 61–68, http://dx.doi.org/10.1007/s100520050513, arXiv:hep-ph/9807297.
[44] S. Chatrchyan, et al., Measurement of the prompt J/ψ and $\psi(2S)$ polarizations in pp collisions at sqrt(s) = 7 TeV, Phys. Lett. B 727 (2013) 381–402, http://dx.doi.org/10.1016/j.physletb.2013.10.055, arXiv:1307.6070.
[45] B. Abelev, et al., J/ψ polarization in pp collisions at $\sqrt{s} = 7$ TeV, Phys. Rev. Lett. 108 (2012) 082001, http://dx.doi.org/10.1103/PhysRevLett.108.082001, arXiv:1111.1630.
[46] R. Aaij, et al., Measurement of J/ψ polarization in pp collisions at $\sqrt{s} = 7$ TeV, Eur. Phys. J. C 73 (2013) 2631, http://dx.doi.org/10.1140/epjc/s10052-013-2631-3, arXiv:1307.6379.
[47] N. Armesto, A. Dainese, C.A. Salgado, U.A. Wiedemann, Testing the color charge and mass dependence of parton energy loss with heavy-to-light ratios at RHIC and CERN LHC, Phys. Rev. D 71 (2005) 054027, http://dx.doi.org/10.1103/PhysRevD.71.054027, arXiv:hep-ph/0501225.
[48] B. Abelev, et al., Measurement of prompt J/ψ and beauty hadron production cross sections at mid-rapidity in pp collisions at $\sqrt{s} = 7$ TeV, J. High Energy Phys. 1211 (2012) 065, http://dx.doi.org/10.1007/JHEP11(2012)065, arXiv:1205.5880.
[49] R. Aaij, et al., Measurement of J/ψ production in pp collisions at $\sqrt{s} = 2.76$ TeV, J. High Energy Phys. 1302 (2013) 041, http://dx.doi.org/10.1007/JHEP02(2013)041, arXiv:1212.1045.
[50] K. Zhou, N. Xu, P. Zhuang, Quarkonium production and medium effects in high energy nuclear collisions, arXiv:1309.7520.
[51] E. Abbas, et al., J/ψ elliptic flow in Pb–Pb collisions at $\sqrt{s_{NN}} = 2.76$ TeV, Phys. Rev. Lett. 111 (2013) 162301, http://dx.doi.org/10.1103/PhysRevLett.111.162301, arXiv:1303.5880, URL http://link.aps.org/doi/10.1103/PhysRevLett.111.162301.
[52] B.B. Abelev, et al., J/ψ production and nuclear effects in p–Pb collisions at $\sqrt{s_{NN}} = 5.02$ TeV, J. High Energy Phys. 1402 (2014) 073, http://dx.doi.org/10.1007/JHEP02(2014)073, arXiv:1308.6726.
[53] R. Aaij, et al., Study of J/ψ production and cold nuclear matter effects in pPb collisions at $\sqrt{s_{NN}} = 5$ TeV, J. High Energy Phys. 1402 (2014) 072, http://dx.doi.org/10.1007/JHEP02(2014)072, arXiv:1308.6729.

ALICE Collaboration

B. Abelev [bv], J. Adam [al], D. Adamová [cd], M.M. Aggarwal [ch], G. Aglieri Rinella [ah], M. Agnello [cn,de], A.G. Agocs [eb], A. Agostinelli [z], N. Agrawal [as], Z. Ahammed [dx], N. Ahmad [r], A. Ahmad Masoodi [r], I. Ahmed [o], S.U. Ahn [bo], S.A. Ahn [bo], I. Aimo [de,cn], S. Aiola [ec], M. Ajaz [o], A. Akindinov [be], D. Aleksandrov [ct], B. Alessandro [de], D. Alexandre [cv], A. Alici [l,cy], A. Alkin [c], J. Alme [aj], T. Alt [an], V. Altini [ae], S. Altinpinar [q],

I. Altsybeev [dw], C. Alves Garcia Prado [dm], C. Andrei [by], A. Andronic [cq], V. Anguelov [cm], J. Anielski [az], T. Antičić [cr], F. Antinori [db], P. Antonioli [cy], L. Aphecetche [df], H. Appelshäuser [ax], N. Arbor [br], S. Arcelli [z], N. Armesto [p], R. Arnaldi [de], T. Aronsson [ec], I.C. Arsene [u,cq], M. Arslandok [ax], A. Augustinus [ah], R. Averbeck [cq], T.C. Awes [ce], M.D. Azmi [r,cj], M. Bach [an], A. Badalà [da], Y.W. Baek [ao,bq], S. Bagnasco [de], R. Bailhache [ax], V. Bairathi [cl], R. Bala [ck], A. Baldisseri [n], F. Baltasar Dos Santos Pedrosa [ah], J. Bán [bf], R.C. Baral [bh], R. Barbera [aa], F. Barile [ae], G.G. Barnaföldi [eb], L.S. Barnby [cv], V. Barret [bq], J. Bartke [dj], M. Basile [z], N. Bastid [bq], S. Basu [dx], B. Bathen [az], G. Batigne [df], B. Batyunya [bm], P.C. Batzing [u], C. Baumann [ax], I.G. Bearden [ca], H. Beck [ax], C. Bedda [cn], N.K. Behera [as], I. Belikov [ba], F. Bellini [z], R. Bellwied [do], E. Belmont-Moreno [bk], G. Bencedi [eb], S. Beole [y], I. Berceanu [by], A. Bercuci [by], Y. Berdnikov [cf,1], D. Berenyi [eb], M.E. Berger [di], A.A.E. Bergognon [df], R.A. Bertens [bd], D. Berzano [y], L. Betev [ah], A. Bhasin [ck], A.K. Bhati [ch], B. Bhattacharjee [ap], J. Bhom [dt], L. Bianchi [y], N. Bianchi [bs], C. Bianchin [bd], J. Bielčík [al], J. Bielčíková [cd], A. Bilandzic [ca], S. Bjelogrlic [bd], F. Blanco [j], D. Blau [ct], C. Blume [ax], F. Bock [bu,cm], F.V. Boehmer [di], A. Bogdanov [bw], H. Bøggild [ca], M. Bogolyubsky [bb], L. Boldizsár [eb], M. Bombara [am], J. Book [ax], H. Borel [n], A. Borissov [cp,ea], J. Bornschein [an], F. Bossú [bl], M. Botje [cb], E. Botta [y], S. Böttger [aw], P. Braun-Munzinger [cq], M. Bregant [dm,df], T. Breitner [aw], T.A. Broker [ax], T.A. Browning [co], M. Broz [ak], E. Bruna [de], G.E. Bruno [ae], D. Budnikov [cs], H. Buesching [ax], S. Bufalino [de], P. Buncic [ah], O. Busch [cm], Z. Buthelezi [bl], D. Caffarri [ab], X. Cai [g], H. Caines [ec], A. Caliva [bd], E. Calvo Villar [cw], P. Camerini [x], V. Canoa Roman [ah], F. Carena [ah], W. Carena [ah], F. Carminati [ah], A. Casanova Díaz [bs], J. Castillo Castellanos [n], E.A.R. Casula [w], V. Catanescu [by], C. Cavicchioli [ah], C. Ceballos Sanchez [i], J. Cepila [al], P. Cerello [de], B. Chang [dp], S. Chapeland [ah], J.L. Charvet [n], S. Chattopadhyay [dx], S. Chattopadhyay [cu], M. Cherney [cg], C. Cheshkov [dv], B. Cheynis [dv], V. Chibante Barroso [ah], D.D. Chinellato [do,dn], P. Chochula [ah], M. Chojnacki [ca], S. Choudhury [dx], P. Christakoglou [cb], C.H. Christensen [ca], P. Christiansen [af], T. Chujo [dt], S.U. Chung [cp], C. Cicalo [cz], L. Cifarelli [l,z], F. Cindolo [cy], J. Cleymans [cj], F. Colamaria [ae], D. Colella [ae], A. Collu [w], M. Colocci [z], G. Conesa Balbastre [br], Z. Conesa del Valle [av,ah], M.E. Connors [ec], G. Contin [x], J.G. Contreras [k], T.M. Cormier [ce,ea], Y. Corrales Morales [y], P. Cortese [ad], I. Cortés Maldonado [b], M.R. Cosentino [bu,dm], F. Costa [ah], P. Crochet [bq], R. Cruz Albino [k], E. Cuautle [bj], L. Cunqueiro [bs,ah], A. Dainese [db], R. Dang [g], A. Danu [bi], D. Das [cu], I. Das [av], K. Das [cu], S. Das [d], A. Dash [dn], S. Dash [as], S. De [dx], H. Delagrange [df,2], A. Deloff [bx], E. Dénes [eb], G. D'Erasmo [ae], G.O.V. de Barros [dm], A. De Caro [l,ac], G. de Cataldo [cx], J. de Cuveland [an], A. De Falco [w], D. De Gruttola [ac,l], N. De Marco [de], S. De Pasquale [ac], R. de Rooij [bd], M.A. Diaz Corchero [j], T. Dietel [az,cj], R. Divià [ah], D. Di Bari [ae], S. Di Liberto [dc], A. Di Mauro [ah], P. Di Nezza [bs], Ø. Djuvsland [q], A. Dobrin [bd,ea], T. Dobrowolski [bx], D. Domenicis Gimenez [dm], B. Dönigus [ax], O. Dordic [u], S. Dorheim [di], A.K. Dubey [dx], A. Dubla [bd], L. Ducroux [dv], P. Dupieux [bq], A.K. Dutta Majumdar [cu], D. Elia [cx], H. Engel [aw], B. Erazmus [ah,df], H.A. Erdal [aj], D. Eschweiler [an], B. Espagnon [av], M. Estienne [df], S. Esumi [dt], D. Evans [cv], S. Evdokimov [bb], G. Eyyubova [u], D. Fabris [db], J. Faivre [br], D. Falchieri [z], A. Fantoni [bs], M. Fasel [cm], D. Fehlker [q], L. Feldkamp [az], D. Felea [bi], A. Feliciello [de], G. Feofilov [dw], J. Ferencei [cd], A. Fernández Téllez [b], E.G. Ferreiro [p], A. Ferretti [y], A. Festanti [ab], J. Figiel [dj], M.A.S. Figueredo [dm,dq], S. Filchagin [cs], D. Finogeev [bc], F.M. Fionda [ae], E.M. Fiore [ae], E. Floratos [ci], M. Floris [ah], S. Foertsch [bl], P. Foka [cq], S. Fokin [ct], E. Fragiacomo [dd], A. Francescon [ab,ah], U. Frankenfeld [cq], U. Fuchs [ah], C. Furget [br], M. Fusco Girard [ac], J.J. Gaardhøje [ca], M. Gagliardi [y], M. Gallio [y], D.R. Gangadharan [s,bu], P. Ganoti [ce,ci], C. Garabatos [cq], E. Garcia-Solis [m], C. Gargiulo [ah], I. Garishvili [bv], J. Gerhard [an], M. Germain [df], A. Gheata [ah], M. Gheata [ah,bi], B. Ghidini [ae], P. Ghosh [dx], S.K. Ghosh [d], P. Gianotti [bs], P. Giubellino [ah], E. Gladysz-Dziadus [dj], P. Glässel [cm], R. Gomez [k], P. González-Zamora [j], S. Gorbunov [an], L. Görlich [dj], S. Gotovac [dh], L.K. Graczykowski [dz], R. Grajcarek [cm], A. Grelli [bd], A. Grigoras [ah], C. Grigoras [ah], V. Grigoriev [bw], A. Grigoryan [a], S. Grigoryan [bm], B. Grinyov [c], N. Grion [dd], J.F. Grosse-Oetringhaus [ah], J.-Y. Grossiord [dv], R. Grosso [ah], F. Guber [bc], R. Guernane [br], B. Guerzoni [z], M. Guilbaud [dv], K. Gulbrandsen [ca], H. Gulkanyan [a], T. Gunji [ds], A. Gupta [ck], R. Gupta [ck], K.H. Khan [o], R. Haake [az], Ø. Haaland [q], C. Hadjidakis [av], M. Haiduc [bi], H. Hamagaki [ds], G. Hamar [eb], L.D. Hanratty [cv], A. Hansen [ca], J.W. Harris [ec], H. Hartmann [an], A. Harton [m], D. Hatzifotiadou [cy], S. Hayashi [ds], A. Hayrapetyan [ah,a], S.T. Heckel [ax], M. Heide [az], H. Helstrup [aj], A. Herghelegiu [by], G. Herrera Corral [k], B.A. Hess [ag], K.F. Hetland [aj], B. Hicks [ec], B. Hippolyte [ba], J. Hladky [bg], P. Hristov [ah], M. Huang [q], T.J. Humanic [s], D. Hutter [an], D.S. Hwang [t], J.-C. Ianigro [dv], R. Ilkaev [cs], I. Ilkiv [bx], M. Inaba [dt], E. Incani [w], G.M. Innocenti [y], C. Ionita [ah], M. Ippolitov [ct], M. Irfan [r], M. Ivanov [cq], V. Ivanov [cf], O. Ivanytskyi [c], A. Jachołkowski [aa], C. Jahnke [dm], H.J. Jang [bo], M.A. Janik [dz], P.H.S.Y. Jayarathna [do],

S. Jena [as,do], R.T. Jimenez Bustamante [bj], P.G. Jones [cv], H. Jung [ao], A. Jusko [cv], S. Kalcher [an], P. Kalinak [bf], A. Kalweit [ah], J. Kamin [ax], J.H. Kang [ed], V. Kaplin [bw], S. Kar [dx], A. Karasu Uysal [bp], O. Karavichev [bc], T. Karavicheva [bc], E. Karpechev [bc], U. Kebschull [aw], R. Keidel [ee], B. Ketzer [ai,di], M.M. Khan [r,3], P. Khan [cu], S.A. Khan [dx], A. Khanzadeev [cf], Y. Kharlov [bb], B. Kileng [aj], B. Kim [ed], D.W. Kim [bo,ao], D.J. Kim [dp], J.S. Kim [ao], M. Kim [ao], M. Kim [ed], S. Kim [t], T. Kim [ed], S. Kirsch [an], I. Kisel [an], S. Kiselev [be], A. Kisiel [dz], G. Kiss [eb], J.L. Klay [f], J. Klein [cm], C. Klein-Bösing [az], A. Kluge [ah], M.L. Knichel [cq], A.G. Knospe [dk], C. Kobdaj [dg,ah], M.K. Köhler [cq], T. Kollegger [an], A. Kolojvari [dw], V. Kondratiev [dw], N. Kondratyeva [bw], A. Konevskikh [bc], V. Kovalenko [dw], M. Kowalski [dj], S. Kox [br], G. Koyithatta Meethaleveedu [as], J. Kral [dp], I. Králik [bf], F. Kramer [ax], A. Kravčáková [am], M. Krelina [al], M. Kretz [an], M. Krivda [cv,bf], F. Krizek [cd,aq], M. Krus [al], E. Kryshen [cf,ah], M. Krzewicki [cq], V. Kučera [cd], Y. Kucheriaev [ct], T. Kugathasan [ah], C. Kuhn [ba], P.G. Kuijer [cb], I. Kulakov [ax], J. Kumar [as], P. Kurashvili [bx], A. Kurepin [bc], A.B. Kurepin [bc], A. Kuryakin [cs], S. Kushpil [cd], V. Kushpil [cd], M.J. Kweon [cm,au], Y. Kwon [ed], P. Ladron de Guevara [bj], C. Lagana Fernandes [dm], I. Lakomov [av], R. Langoy [dy], C. Lara [aw], A. Lardeux [df], A. Lattuca [y], S.L. La Pointe [bd,de], P. La Rocca [aa], R. Lea [x], G.R. Lee [cv], I. Legrand [ah], J. Lehnert [ax], R.C. Lemmon [cc], M. Lenhardt [cq], V. Lenti [cx], E. Leogrande [bd], M. Leoncino [y], I. León Monzón [dl], P. Lévai [eb], S. Li [bq,g], J. Lien [dy,q], R. Lietava [cv], S. Lindal [u], V. Lindenstruth [an], C. Lippmann [cq], M.A. Lisa [s], H.M. Ljunggren [af], D.F. Lodato [bd], P.I. Loenne [q], V.R. Loggins [ea], V. Loginov [bw], D. Lohner [cm], C. Loizides [bu], X. Lopez [bq], E. López Torres [i], X.-G. Lu [cm], P. Luettig [ax], M. Lunardon [ab], J. Luo [g], G. Luparello [bd], C. Luzzi [ah], A.M. Gago [cw], P.M. Jacobs [bu], R. Ma [ec], A. Maevskaya [bc], M. Mager [ah], D.P. Mahapatra [bh], A. Maire [cm,ba], M. Malaev [cf], I. Maldonado Cervantes [bj], L. Malinina [bm,4], D. Mal'Kevich [be], P. Malzacher [cq], A. Mamonov [cs], L. Manceau [de], V. Manko [ct], F. Manso [bq], V. Manzari [cx,ah], M. Marchisone [bq,y], J. Mareš [bg], G.V. Margagliotti [x], A. Margotti [cy], A. Marín [cq], C. Markert [ah,dk], M. Marquard [ax], I. Martashvili [dr], N.A. Martin [cq], P. Martinengo [ah], M.I. Martínez [b], G. Martínez García [df], J. Martin Blanco [df], Y. Martynov [c], A. Mas [df], S. Masciocchi [cq], M. Masera [y], A. Masoni [cz], L. Massacrier [df], A. Mastroserio [ae], A. Matyja [dj], C. Mayer [dj], J. Mazer [dr], R. Mazumder [at], M.A. Mazzoni [dc], F. Meddi [v], A. Menchaca-Rocha [bk], J. Mercado Pérez [cm], M. Meres [ak], Y. Miake [dt], K. Mikhaylov [be,bm], L. Milano [ah], J. Milosevic [u,5], A. Mischke [bd], A.N. Mishra [at], D. Miśkowiec [cq], C.M. Mitu [bi], J. Mlynarz [ea], B. Mohanty [dx,bz], L. Molnar [ba], L. Montaño Zetina [k], E. Montes [j], M. Morando [ab], D.A. Moreira De Godoy [dm], S. Moretto [ab], A. Morreale [dp,df], A. Morsch [ah], V. Muccifora [bs], E. Mudnic [dh], S. Muhuri [dx], M. Mukherjee [dx], H. Müller [ah], M.G. Munhoz [dm], S. Murray [cj,bl], L. Musa [ah], J. Musinsky [bf], B.K. Nandi [as], R. Nania [cy], E. Nappi [cx], C. Nattrass [dr], T.K. Nayak [dx], S. Nazarenko [cs], A. Nedosekin [be], M. Nicassio [cq], M. Niculescu [ah,bi], B.S. Nielsen [ca], S. Nikolaev [ct], S. Nikulin [ct], V. Nikulin [cf], B.S. Nilsen [cg], F. Noferini [l,cy], P. Nomokonov [bm], G. Nooren [bd], A. Nyanin [ct], A. Nyatha [as], J. Nystrand [q], H. Oeschler [cm,ay], S. Oh [ec], S.K. Oh [bn,ao,6], A. Okatan [bp], L. Olah [eb], J. Oleniacz [dz], A.C. Oliveira Da Silva [dm], J. Onderwaater [cq], C. Oppedisano [de], A. Ortiz Velasquez [af], A. Oskarsson [af], J. Otwinowski [cq], K. Oyama [cm], Y. Pachmayer [cm], M. Pachr [al], P. Pagano [ac], G. Paić [bj], F. Painke [an], C. Pajares [p], S.K. Pal [dx], A. Palmeri [da], D. Pant [as], V. Papikyan [a], G.S. Pappalardo [da], W.J. Park [cq], A. Passfeld [az], D.I. Patalakha [bb], V. Paticchio [cx], B. Paul [cu], T. Pawlak [dz], T. Peitzmann [bd], H. Pereira Da Costa [n], E. Pereira De Oliveira Filho [dm], D. Peresunko [ct], C.E. Pérez Lara [cb], W. Peryt [dz,2], A. Pesci [cy], Y. Pestov [e], V. Petráček [al], M. Petran [al], M. Petris [by], M. Petrovici [by], C. Petta [aa], S. Piano [dd], M. Pikna [ak], P. Pillot [df], O. Pinazza [ah,cy], L. Pinsky [do], D.B. Piyarathna [do], M. Planinic [cr,du], M. Płoskoń [bu], J. Pluta [dz], S. Pochybova [eb], P.L.M. Podesta-Lerma [dl], M.G. Poghosyan [ah,cg], E.H.O. Pohjoisaho [aq], B. Polichtchouk [bb], N. Poljak [cr,du], A. Pop [by], S. Porteboeuf-Houssais [bq], J. Porter [bu], V. Pospisil [al], B. Potukuchi [ck], S.K. Prasad [ea,d], R. Preghenella [cy,l], F. Prino [de], C.A. Pruneau [ea], I. Pshenichnov [bc], G. Puddu [w], P. Pujahari [ea,as], V. Punin [cs], J. Putschke [ea], H. Qvigstad [u], A. Rachevski [dd], S. Raha [d], J. Rak [dp], A. Rakotozafindrabe [n], L. Ramello [ad], R. Raniwala [cl], S. Raniwala [cl], S.S. Räsänen [aq], B.T. Rascanu [ax], D. Rathee [ch], A.W. Rauf [o], V. Razazi [w], K.F. Read [dr], J.S. Real [br], K. Redlich [bx,7], R.J. Reed [ec], A. Rehman [q], P. Reichelt [ax], M. Reicher [bd], F. Reidt [ah], R. Renfordt [ax], A.R. Reolon [bs], A. Reshetin [bc], F. Rettig [an], J.-P. Revol [ah], K. Reygers [cm], V. Riabov [cf], R.A. Ricci [bt], T. Richert [af], M. Richter [u], P. Riedler [ah], W. Riegler [ah], F. Riggi [aa], A. Rivetti [de], E. Rocco [bd], M. Rodríguez Cahuantzi [b], A. Rodriguez Manso [cb], K. Røed [u], E. Rogochaya [bm], S. Rohni [ck], D. Rohr [an], D. Röhrich [q], R. Romita [dq,cc], F. Ronchetti [bs], L. Ronflette [df], P. Rosnet [bq], S. Rossegger [ah], A. Rossi [ah], A. Roy [at], C. Roy [ba], P. Roy [cu], A.J. Rubio Montero [j], R. Rui [x], R. Russo [y], E. Ryabinkin [ct], Y. Ryabov [cf], A. Rybicki [dj], S. Sadovsky [bb], K. Šafařík [ah], B. Sahlmuller [ax], R. Sahoo [at], P.K. Sahu [bh], J. Saini [dx], C.A. Salgado [p], J. Salzwedel [s], S. Sambyal [ck], V. Samsonov [cf],

X. Sanchez Castro [ba,bj], F.J. Sánchez Rodríguez [dl], L. Šándor [bf], A. Sandoval [bk], M. Sano [dt], G. Santagati [aa], D. Sarkar [dx], E. Scapparone [cy], F. Scarlassara [ab], R.P. Scharenberg [co], C. Schiaua [by], R. Schicker [cm], C. Schmidt [cq], H.R. Schmidt [ag], S. Schuchmann [ax], J. Schukraft [ah], M. Schulc [al], T. Schuster [ec], Y. Schutz [ah,df], K. Schwarz [cq], K. Schweda [cq], G. Scioli [z], E. Scomparin [de], P.A. Scott [cv], R. Scott [dr], G. Segato [ab], J.E. Seger [cg], I. Selyuzhenkov [cq], J. Seo [cp], E. Serradilla [j,bk], A. Sevcenco [bi], A. Shabetai [df], G. Shabratova [bm], R. Shahoyan [ah], A. Shangaraev [bb], N. Sharma [dr,bh], S. Sharma [ck], K. Shigaki [ar], K. Shtejer [y], Y. Sibiriak [ct], S. Siddhanta [cz], T. Siemiarczuk [bx], D. Silvermyr [ce], C. Silvestre [br], G. Simatovic [du], R. Singaraju [dx], R. Singh [ck], S. Singha [bz,dx], V. Singhal [dx], B.C. Sinha [dx], T. Sinha [cu], B. Sitar [ak], M. Sitta [ad], T.B. Skaali [u], K. Skjerdal [q], R. Smakal [al], N. Smirnov [ec], R.J.M. Snellings [bd], C. Søgaard [af], R. Soltz [bv], J. Song [cp], M. Song [ed], F. Soramel [ab], S. Sorensen [dr], M. Spacek [al], I. Sputowska [dj], M. Spyropoulou-Stassinaki [ci], B.K. Srivastava [co], J. Stachel [cm], I. Stan [bi], G. Stefanek [bx], M. Steinpreis [s], E. Stenlund [af], G. Steyn [bl], J.H. Stiller [cm], D. Stocco [df], M. Stolpovskiy [bb], P. Strmen [ak], A.A.P. Suaide [dm], M.A. Subieta Vasquez [y], T. Sugitate [ar], C. Suire [av], M. Suleymanov [o], R. Sultanov [be], M. Šumbera [cd], T. Susa [cr], T.J.M. Symons [bu], A. Szanto de Toledo [dm], I. Szarka [ak], A. Szczepankiewicz [ah], M. Szymanski [dz], J. Takahashi [dn], M.A. Tangaro [ae], J.D. Tapia Takaki [av,8], A. Tarantola Peloni [ax], A. Tarazona Martinez [ah], A. Tauro [ah], G. Tejeda Muñoz [b], A. Telesca [ah], C. Terrevoli [ae], A. Ter Minasyan [ct,bw], J. Thäder [cq], D. Thomas [bd], R. Tieulent [dv], A.R. Timmins [do], A. Toia [db,ax], H. Torii [ds], V. Trubnikov [c], W.H. Trzaska [dp], T. Tsuji [ds], A. Tumkin [cs], R. Turrisi [db], T.S. Tveter [u], J. Ulery [ax], K. Ullaland [q], J. Ulrich [aw], A. Uras [dv], G.L. Usai [w], M. Vajzer [cd], M. Vala [bf,bm], L. Valencia Palomo [bq,av], S. Vallero [y,cm], P. Vande Vyvre [ah], L. Vannucci [bt], J.W. Van Hoorne [ah], M. van Leeuwen [bd], A. Vargas [b], R. Varma [as], M. Vasileiou [ci], A. Vasiliev [ct], V. Vechernin [dw], M. Veldhoen [bd], M. Venaruzzo [x], E. Vercellin [y], S. Vergara Limón [b], R. Vernet [h], M. Verweij [ea], L. Vickovic [dh], G. Viesti [ab], J. Viinikainen [dp], Z. Vilakazi [bl], O. Villalobos Baillie [cv], A. Vinogradov [ct], L. Vinogradov [dw], Y. Vinogradov [cs], T. Virgili [ac], Y.P. Viyogi [dx], A. Vodopyanov [bm], M.A. Völkl [cm], K. Voloshin [be], S.A. Voloshin [ea], G. Volpe [ah], B. von Haller [ah], I. Vorobyev [dw], D. Vranic [cq,ah], J. Vrláková [am], B. Vulpescu [bq], A. Vyushin [cs], B. Wagner [q], J. Wagner [cq], V. Wagner [al], M. Wang [g,df], Y. Wang [cm], D. Watanabe [dt], M. Weber [do], J.P. Wessels [az], U. Westerhoff [az], J. Wiechula [ag], J. Wikne [u], M. Wilde [az], G. Wilk [bx], J. Wilkinson [cm], M.C.S. Williams [cy], B. Windelband [cm], M. Winn [cm], C. Xiang [g], C.G. Yaldo [ea], Y. Yamaguchi [ds], H. Yang [n,bd], P. Yang [g], S. Yang [q], S. Yano [ar], S. Yasnopolskiy [ct], J. Yi [cp], Z. Yin [g], I.-K. Yoo [cp], I. Yushmanov [ct], V. Zaccolo [ca], C. Zach [al], A. Zaman [o], C. Zampolli [cy], S. Zaporozhets [bm], A. Zarochentsev [dw], P. Závada [bg], N. Zaviyalov [cs], H. Zbroszczyk [dz], I.S. Zgura [bi], M. Zhalov [cf], F. Zhang [g], H. Zhang [g], X. Zhang [bq,g,bu], Y. Zhang [g], C. Zhao [u], D. Zhou [g], F. Zhou [g], Y. Zhou [bd], H. Zhu [g], J. Zhu [g], J. Zhu [g], X. Zhu [g], A. Zichichi [l,z], A. Zimmermann [cm], M.B. Zimmermann [ah,az], G. Zinovjev [c], Y. Zoccarato [dv], M. Zynovyev [c], M. Zyzak [ax]

[a] *A.I. Alikhanyan National Science Laboratory (Yerevan Physics Institute) Foundation, Yerevan, Armenia*
[b] *Benemérita Universidad Autónoma de Puebla, Puebla, Mexico*
[c] *Bogolyubov Institute for Theoretical Physics, Kiev, Ukraine*
[d] *Bose Institute, Department of Physics and Centre for Astroparticle Physics and Space Science (CAPSS), Kolkata, India*
[e] *Budker Institute for Nuclear Physics, Novosibirsk, Russia*
[f] *California Polytechnic State University, San Luis Obispo, CA, United States*
[g] *Central China Normal University, Wuhan, China*
[h] *Centre de Calcul de l'IN2P3, Villeurbanne, France*
[i] *Centro de Aplicaciones Tecnológicas y Desarrollo Nuclear (CEADEN), Havana, Cuba*
[j] *Centro de Investigaciones Energéticas Medioambientales y Tecnológicas (CIEMAT), Madrid, Spain*
[k] *Centro de Investigación y de Estudios Avanzados (CINVESTAV), Mexico City and Mérida, Mexico*
[l] *Centro Fermi – Museo Storico della Fisica e Centro Studi e Ricerche "Enrico Fermi", Rome, Italy*
[m] *Chicago State University, Chicago, USA*
[n] *Commissariat à l'Energie Atomique, IRFU, Saclay, France*
[o] *COMSATS Institute of Information Technology (CIIT), Islamabad, Pakistan*
[p] *Departamento de Física de Partículas and IGFAE, Universidad de Santiago de Compostela, Santiago de Compostela, Spain*
[q] *Department of Physics and Technology, University of Bergen, Bergen, Norway*
[r] *Department of Physics, Aligarh Muslim University, Aligarh, India*
[s] *Department of Physics, Ohio State University, Columbus, OH, United States*
[t] *Department of Physics, Sejong University, Seoul, South Korea*
[u] *Department of Physics, University of Oslo, Oslo, Norway*
[v] *Dipartimento di Fisica dell'Università 'La Sapienza' and Sezione INFN Rome*
[w] *Dipartimento di Fisica dell'Università and Sezione INFN, Cagliari, Italy*
[x] *Dipartimento di Fisica dell'Università and Sezione INFN, Trieste, Italy*
[y] *Dipartimento di Fisica dell'Università and Sezione INFN, Turin, Italy*
[z] *Dipartimento di Fisica e Astronomia dell'Università and Sezione INFN, Bologna, Italy*
[aa] *Dipartimento di Fisica e Astronomia dell'Università and Sezione INFN, Catania, Italy*
[ab] *Dipartimento di Fisica e Astronomia dell'Università and Sezione INFN, Padova, Italy*
[ac] *Dipartimento di Fisica 'E.R. Caianiello' dell'Università and Gruppo Collegato INFN, Salerno, Italy*
[ad] *Dipartimento di Scienze e Innovazione Tecnologica dell'Università del Piemonte Orientale and Gruppo Collegato INFN, Alessandria, Italy*

[ae] Dipartimento Interateneo di Fisica 'M. Merlin' and Sezione INFN, Bari, Italy
[af] Division of Experimental High Energy Physics, University of Lund, Lund, Sweden
[ag] Eberhard Karls Universität Tübingen, Tübingen, Germany
[ah] European Organization for Nuclear Research (CERN), Geneva, Switzerland
[ai] Excellence Cluster Universe, Technische Universität München, Munich, Germany
[aj] Faculty of Engineering, Bergen University College, Bergen, Norway
[ak] Faculty of Mathematics, Physics and Informatics, Comenius University, Bratislava, Slovakia
[al] Faculty of Nuclear Sciences and Physical Engineering, Czech Technical University in Prague, Prague, Czech Republic
[am] Faculty of Science, P.J. Šafárik University, Košice, Slovakia
[an] Frankfurt Institute for Advanced Studies, Johann Wolfgang Goethe-Universität Frankfurt, Frankfurt, Germany
[ao] Gangneung-Wonju National University, Gangneung, South Korea
[ap] Gauhati University, Department of Physics, Guwahati, India
[aq] Helsinki Institute of Physics (HIP), Helsinki, Finland
[ar] Hiroshima University, Hiroshima, Japan
[as] Indian Institute of Technology Bombay (IIT), Mumbai, India
[at] Indian Institute of Technology Indore (IITI), Indore, India
[au] Inha University, College of Natural Sciences, South Korea
[av] Institut de Physique Nucleaire d'Orsay (IPNO), Universite Paris-Sud, CNRS-IN2P3, Orsay, France
[aw] Institut für Informatik, Johann Wolfgang Goethe-Universität Frankfurt, Frankfurt, Germany
[ax] Institut für Kernphysik, Johann Wolfgang Goethe-Universität Frankfurt, Frankfurt, Germany
[ay] Institut für Kernphysik, Technische Universität Darmstadt, Darmstadt, Germany
[az] Institut für Kernphysik, Westfälische Wilhelms-Universität Münster, Münster, Germany
[ba] Institut Pluridisciplinaire Hubert Curien (IPHC), Université de Strasbourg, CNRS-IN2P3, Strasbourg, France
[bb] Institute for High Energy Physics, Protvino, Russia
[bc] Institute for Nuclear Research, Academy of Sciences, Moscow, Russia
[bd] Institute for Subatomic Physics of Utrecht University, Utrecht, Netherlands
[be] Institute for Theoretical and Experimental Physics, Moscow, Russia
[bf] Institute of Experimental Physics, Slovak Academy of Sciences, Košice, Slovakia
[bg] Institute of Physics, Academy of Sciences of the Czech Republic, Prague, Czech Republic
[bh] Institute of Physics, Bhubaneswar, India
[bi] Institute of Space Science (ISS), Bucharest, Romania
[bj] Instituto de Ciencias Nucleares, Universidad Nacional Autónoma de México, Mexico City, Mexico
[bk] Instituto de Física, Universidad Nacional Autónoma de México, Mexico City, Mexico
[bl] iThemba LABS, National Research Foundation, Somerset West, South Africa
[bm] Joint Institute for Nuclear Research (JINR), Dubna, Russia
[bn] Konkuk University, Seoul, South Korea
[bo] Korea Institute of Science and Technology Information, Daejeon, South Korea
[bp] KTO Karatay University, Konya, Turkey
[bq] Laboratoire de Physique Corpusculaire (LPC), Clermont Université, Université Blaise Pascal, CNRS-IN2P3, Clermont-Ferrand, France
[br] Laboratoire de Physique Subatomique et de Cosmologie (LPSC), Université Joseph Fourier, CNRS-IN2P3, Institut Polytechnique de Grenoble, Grenoble, France
[bs] Laboratori Nazionali di Frascati, INFN, Frascati, Italy
[bt] Laboratori Nazionali di Legnaro, INFN, Legnaro, Italy
[bu] Lawrence Berkeley National Laboratory, Berkeley, CA, United States
[bv] Lawrence Livermore National Laboratory, Livermore, CA, United States
[bw] Moscow Engineering Physics Institute, Moscow, Russia
[bx] National Centre for Nuclear Studies, Warsaw, Poland
[by] National Institute for Physics and Nuclear Engineering, Bucharest, Romania
[bz] National Institute of Science Education and Research, Bhubaneswar, India
[ca] Niels Bohr Institute, University of Copenhagen, Copenhagen, Denmark
[cb] Nikhef, National Institute for Subatomic Physics, Amsterdam, Netherlands
[cc] Nuclear Physics Group, STFC Daresbury Laboratory, Daresbury, United Kingdom
[cd] Nuclear Physics Institute, Academy of Sciences of the Czech Republic, Řež u Prahy, Czech Republic
[ce] Oak Ridge National Laboratory, Oak Ridge, TN, United States
[cf] Petersburg Nuclear Physics Institute, Gatchina, Russia
[cg] Physics Department, Creighton University, Omaha, NE, United States
[ch] Physics Department, Panjab University, Chandigarh, India
[ci] Physics Department, University of Athens, Athens, Greece
[cj] Physics Department, University of Cape Town, Cape Town, South Africa
[ck] Physics Department, University of Jammu, Jammu, India
[cl] Physics Department, University of Rajasthan, Jaipur, India
[cm] Physikalisches Institut, Ruprecht-Karls-Universität Heidelberg, Heidelberg, Germany
[cn] Politecnico di Torino, Turin, Italy
[co] Purdue University, West Lafayette, IN, United States
[cp] Pusan National University, Pusan, South Korea
[cq] Research Division and ExtreMe Matter Institute EMMI, GSI Helmholtzzentrum für Schwerionenforschung, Darmstadt, Germany
[cr] Rudjer Bošković Institute, Zagreb, Croatia
[cs] Russian Federal Nuclear Center (VNIIEF), Sarov, Russia
[ct] Russian Research Centre Kurchatov Institute, Moscow, Russia
[cu] Saha Institute of Nuclear Physics, Kolkata, India
[cv] School of Physics and Astronomy, University of Birmingham, Birmingham, United Kingdom
[cw] Sección Física, Departamento de Ciencias, Pontificia Universidad Católica del Perú, Lima, Peru
[cx] Sezione INFN, Bari, Italy
[cy] Sezione INFN, Bologna, Italy
[cz] Sezione INFN, Cagliari, Italy
[da] Sezione INFN, Catania, Italy
[db] Sezione INFN, Padova, Italy
[dc] Sezione INFN, Rome, Italy
[dd] Sezione INFN, Trieste, Italy
[de] Sezione INFN, Turin, Italy

[df] *SUBATECH, Ecole des Mines de Nantes, Université de Nantes, CNRS-IN2P3, Nantes, France*
[dg] *Suranaree University of Technology, Nakhon Ratchasima, Thailand*
[dh] *Technical University of Split FESB, Split, Croatia*
[di] *Technische Universität München, Munich, Germany*
[dj] *The Henryk Niewodniczanski Institute of Nuclear Physics, Polish Academy of Sciences, Cracow, Poland*
[dk] *The University of Texas at Austin, Physics Department, Austin, TX, USA*
[dl] *Universidad Autónoma de Sinaloa, Culiacán, Mexico*
[dm] *Universidade de São Paulo (USP), São Paulo, Brazil*
[dn] *Universidade Estadual de Campinas (UNICAMP), Campinas, Brazil*
[do] *University of Houston, Houston, TX, United States*
[dp] *University of Jyväskylä, Jyväskylä, Finland*
[dq] *University of Liverpool, Liverpool, United Kingdom*
[dr] *University of Tennessee, Knoxville, TN, United States*
[ds] *University of Tokyo, Tokyo, Japan*
[dt] *University of Tsukuba, Tsukuba, Japan*
[du] *University of Zagreb, Zagreb, Croatia*
[dv] *Université de Lyon, Université Lyon 1, CNRS/IN2P3, IPN-Lyon, Villeurbanne, France*
[dw] *V. Fock Institute for Physics, St. Petersburg State University, St. Petersburg, Russia*
[dx] *Variable Energy Cyclotron Centre, Kolkata, India*
[dy] *Vestfold University College, Tonsberg, Norway*
[dz] *Warsaw University of Technology, Warsaw, Poland*
[ea] *Wayne State University, Detroit, MI, United States*
[eb] *Wigner Research Centre for Physics, Hungarian Academy of Sciences, Budapest, Hungary*
[ec] *Yale University, New Haven, CT, United States*
[ed] *Yonsei University, Seoul, South Korea*
[ee] *Zentrum für Technologietransfer und Telekommunikation (ZTT), Fachhochschule Worms, Worms, Germany*

[1] St. Petersburg State Polytechnical University.
[2] Deceased.
[3] Department of Applied Physics, Aligarh Muslim University, Aligarh, India.
[4] M.V. Lomonosov Moscow State University, D.V. Skobeltsyn Institute of Nuclear Physics, Moscow, Russia.
[5] University of Belgrade, Faculty of Physics and "Vinča" Institute of Nuclear Sciences, Belgrade, Serbia.
[6] Konkuk University, Seoul, South Korea.
[7] Institute of Theoretical Physics, University of Wroclaw, Wroclaw, Poland.
[8] The University of Kansas, Lawrence, KS, United States.